

Imperfections in Reaction Diffusion Simulations

Dennis Barzanoff

22nd March 2024

Supervisor: James Stovold

B.Sc. (Hons) Computer Science

Number of words = 8542

This includes the body of the report only

Declaration of Originality

I certify that the material contained in this dissertation is my own work and does not contain unreferenced or unacknowledged material. I also warrant that the above statement applies to the implementation of the project and all associated documentation. Regarding the electronically submitted work, I consent to this being stored electronically and copied for assessment purposes, including the School's use of plagiarism detection systems in order to check the integrity of assessed work.

I agree to my dissertation being placed in the public domain, with my name explicitly included as the author of the work.

Name: Dennis Barzanoff

Date: 22nd March 2024

Abstract

The project aims to explore how changes in light imperfections impact the realism of a BZ simulation as it's scaled in size. The code is in Metal/GPU and runs experiments varying different simulation parameters that correspond to real-world changes, and then measures results. Changes in light were found to significantly impact the correct behaviour of BZ computer simulations and more advanced light management tools such as LED panels are required to scale large BZ circuits.

Contents

1	Introduction	1
1.1	Chemical Computer	1
1.2	Document Structure	1
1.3	Motivation	1
1.4	Scope of the Dissertation	2
1.4.1	Chemical Computer Size Limitations	2
1.4.2	Investigating the Effects of Imperfections on Illumination Uniformity	2
1.4.3	Estimating the Maximum Size of the Chemical Computer	3
1.4.4	Recreating Stovold and O'Keefe (2017) In Real Life	3
1.4.5	Impact of Reflection And Refraction on Light Loss	3
1.4.6	Impact of OHP Sheet Thickness on Light Absorption	3
2	Background & Literature Review	4
2.1	Reaction Diffusion	4
2.2	Belousov-Zhabotinsky Reaction	4
2.3	Chemical Computing	5
2.4	Oregonator Model	5
2.4.1	The Mathematics Behind the Oregonator Model	5
2.5	Motivation	6
2.6	Goals & Objectives	7
3	Design & Implementation	8
4	Results	10
4.1	Creating a Coincidence Detector In Simulation	10
4.1.1	Unsuccessful Detector	10
4.1.2	Successful Detector	12
4.2	Mapping the Simulation Size to Real Life	12
4.3	Finding ϕ_{\min} and ϕ_{\max} for a Chemical Diode	14
4.3.1	Measuring ϕ_{\min} , ϕ_{\max}	15
4.3.2	Propagation Time Variation of the Diode Under Different Lighting Conditions	15
4.3.3	Results	18
4.4	Estimating The Light Source's Position	18
4.5	Estimating The Maximum Petri Dish Size for a Chemical Diode (Gorecki et al., 2003)	24
4.6	Light Impact on a CMM Neural Network (Stovold and O'Keefe, 2017)	28
4.7	Light Impact on a single CMM Neuron (Stovold and O'Keefe, 2017)	29
4.7.1	Testing the Custom CMM Neuron with different values of I_p	30

Contents

5 Conclusion & Future work	31
5.1 Alternative Light Sources	31
5.2 Future Work	31
5.2.1 Accounting for Light Loss Due to Reflection	31
5.2.2 Beer-Lambert Law for Absorption	33
5.2.3 Examining the Impact of Spike on Diode Robustness	34
5.2.4 Accounting for the Change on ϕ_{active}	34
5.2.5 Accounting for Other Chemical Component Limitations Than Diodes	34
A Original Project Proposal	37
A.1 Aims & Objectives	37
A.1.1 Aims	37
A.1.2 Challenges	37
A.2 Related work	38
A.3 Methodologies	38
A.4 Programme of Work	39

List of Figures

1.1	Coincidence detector (AND gate) is a chemical circuit that takes two input signals and only produces an output when both inputs are present at the same time. Note that there is no clock signal, so the inputs must arrive simultaneously for correct operation. (Gorecki et al., 2003)	2
2.1	Time-lapse of the Belousov-Zhabotinsky reaction in a petri dish done in the University of Stavanger	5
2.2	Graphical representation of the function $\frac{u-q}{u+q}$ showing how it influences the reaction rate in the Oregonator model	7
3.1	The Metal Dependency Pipeline consists of a Compute Command Encoder (represented by red circles) and a Render Command Encoder (depicted by yellow circles). The Compute Command Encoder is run multiple times, performing as many calculations as possible. Simultaneously, the Render Command Encoder operates periodically to render the computed results. These two encoders work in parallel, with the Render Command Encoder producing output every time it gets a chance, while the Compute Command Encoder continuously performs computations most of the time.	9
4.1	Initial Coincidence Detector Configuration	10
4.2	First Successful Coincidence Detector	12
4.3	First working AND gate	13
4.4	Real-life AND gate using BZ reaction (Gorecki et al., 2003)	14
4.5	Diode Experiment	18
4.6	Propagation times for various ϕ_{passive} values within the limits of ϕ_{\min} and ϕ_{\max} , illustrating the experimental outcomes of testing a diode in a Belousov-Zhabotinsky reaction. Each point represents a propagation time measurement for a given ϕ_{passive} , with the average propagation time across measurements shown by a thicker black line. The shaded area between ϕ_{\min} (red dashed line) and ϕ_{\max} (blue dashed line) highlights the range where the diode works correctly, with the ϕ used commonly in literature marked by a solid green line.	19
4.7	Propagation times around the value of ϕ_{\max} . The range of ϕ is $\phi_{\max} - 7 \times 10^{-6} \leq \phi \leq \phi_{\max} + 3 \times 10^{-6}$	19
4.8	Comparison of two waves passing through a diode. Above $\phi_{\text{passive}} = \phi_{\text{literature}}$, below $\phi_{\text{passive}} = \phi_{\max}$. Both have different propagation speeds, so they have been equalised for the purpose of comparing their interaction with the diode side by side. The second wave takes substantially more time to form and is about 700 time steps slower as seen in Figure 4.7, which is quite a lot in such simulations.	20
4.9	Visualization of light interaction with a Petri dish (Edwards, 1970)	20

List of Figures

4.10 Experimental setup for observing pulses in a photosensitive BZ reaction (Gorecki et al., 2003)	21
4.11 Radius Illumination Graph	23
4.12 Illustration of finding the angle θ	24
4.13 The graph represents the percentage of illumination I_p as a function of the radial distance r_c from the center of the Petri dish. The illumination percentage is calculated using the equation: $I_p = \frac{1}{\sqrt{1+(\frac{r_c}{h})^2}}$ where r_c is the radial distance from the center of the Petri dish in millimeters, and h is the height of the light source above the center of the Petri dish, which is 148 mm. The graph extends from $r_c = -1000$ mm to $r_c = 1000$ mm to illustrate the symmetrical decrease in illumination intensity on both sides of the center point.	25
4.14 The graph illustrates the illumination intensity (ϕ) as a function of radial distance from the center of a Petri dish, represented by an oval at the bottom center. The shaded area within ± 10 mm indicates the physical size of the Petri dish. A movable area of approximately 40.87 mm from the edge of the Petri dish to the radial distance corresponding to ϕ_{min} is highlighted, demonstrating the operational range within which the chemical diode effectively inhibits the reaction. Beyond this range, the diode becomes non-operational, allowing the reaction to proceed unimpeded.	27
4.15 Image of a single neuron cell sized at 116x144px built and tested in our simulation, which will be used as a reference for scaling to the approximate size of a single neuron in Stovold and O'Keefe (2017).	29
A.1 Expanding wave pattern from this project using the Oregonator model	38
A.2 Reaction Diffusion Game by Chaotic Edge	39
A.3 Gantt Chart	40

List of Tables

3.1	Simulation parameters with their respective values.	8
4.1	Results of the experiment showing the relationship between conductor width and gap size.	11

1 Introduction

A chemical computer is a computer that uses chemistry to perform computations. It is a new field of research where rapid innovations have taken place in recent years. The project as a whole aims to explore how different imperfections impact the realism of a chemical computer simulation when it is transferred to the real environment. Imperfections, such as light and temperature changes, are among the most significant factors that can have an effect on the correctness of the computer. Not every piece of information was there to make the conclusions made in the project, but for what was missing, it was made clear using very visible sections for assumptions.

1.1 Chemical Computer

The main idea behind chemical computers is that chemical reactions can be used to do useful things. Most logic gates used in traditional computers can be created in chemical ones too. A popular component for that is the Coincidence Detector (AND gate), shown in Figure 1.1. AND gates produce an output only when both inputs are present at the same time.

1.2 Document Structure

This project is structured in the following way:

- **Introduction** introduces the project and its goals.
- **Background & Literature Review** gives a comprehensive introduction to the concepts of chemical computing and reaction diffusion.
- **Design & Implementation** gives a general overview of the tools and technologies used in the project, however each chapter will have its own section on the process of conducting measurements and calculations.
- **Results** contains the body of the dissertation, where different imperfections are explored and interesting conclusions are reached.
- **Conclusion & Future Work** summarises the findings of the project and gives a direction for possible future work and enhancements.

1.3 Motivation

During the research for the project, it was found that there is a lot of research in the field, some in simulations, others in real life (see Chapter 2). However, there is not much research in between the real-life chemical computers and the simulated ones, leaving many



Figure 1.1: Coincidence detector (AND gate) is a chemical circuit that takes two input signals and only produces an output when both inputs are present at the same time. Note that there is no clock signal, so the inputs must arrive simultaneously for correct operation. (Gorecki et al., 2003)

questions unanswered. These questions are covered in Section 1.4. This project was born in an effort to bridge the gap between the two, and to explore how far off the simulations are from the real world.

1.4 Scope of the Dissertation

The scope revolves around exploring different imperfections that impact simulation realism.

1.4.1 Chemical Computer Size Limitations

Most chemical circuits in real life are done in a petri dish and simulations are done in a 2D grid that represents that petri dish. It is unclear what impact the size of the petri dish has on the performance of the computer. Simulations do not take this into account and assume it works the same with any size. It is also unclear how to recreate a chemical computer from a simulation into a petri dish, namely, the size of the petri dish. This is because the petri dish computer is measured in mm, while the simulation is in pixels. Section 4.2 explores this.

1.4.2 Investigating the Effects of Imperfections on Illumination Uniformity

Chemical computing uses light to mould out circuits where the reactions can operate inside of a small petri dish. Most research uses a constant light source in the form of a halougen light bulb, but this light source is not perfect and does not provide constant illumination across the whole dish. This is done in several sections because they depend on each other.

- (1) **Establishing Computer Limits:** The limits of the computer are established in Section 4.3.
- (2) **Calculating Light Source Position and Imperfections:** The position of the light source is calculated in Section 4.4, along with the imperfections that come with it.

ref

ref image

1.4.3 Estimating the Maximum Size of the Chemical Computer

The Chemical Computer is as big as the petri dish it resides in. It is interesting if there is a maximum size that the computer can be before it stops working and what limits the size of the computer. Using the information detailed in items (1) and (2), the maximum size of the computer is calculated in Section 4.5.

1.4.4 Recreating Stovold and O'Keefe (2017) In Real Life

Stovold and O'Keefe (2017) creates a CMM neuron with a similar simulation to the one used in this project. It is interesting if it is possible to recreate this project in real life. Section 4.6 goes into detail about this using results from the previous sections.

1.4.5 Impact of Reflection And Refraction on Light Loss

The OHP sheet discussed in section 1.4.6 is normally unaffected by light angle because the light bulb shined across the petri dish is directly above it and the angle of the light is very close to 90 degrees. However, as discussed in section 1.4.1, as the circuit is scaled in size, the angle of the light changes and the OHP sheet starts to not let all the light through as some of it reflects away. This is discussed in Section 5.2.1.

1.4.6 Impact of OHP Sheet Thickness on Light Absorption

Chemical circuits done in a petri dish use a thin sheet of plastic to hold the circuit mask in place. Most of it is transparent except for the mask, which is opaque and allows for illumination to impact only the parts of the circuit that are needed to be passive during the reaction. This is talked about in section 5.2.2.

2 Background & Literature Review

This chapter gives an introduction to the concepts of reaction diffusion and chemical computing, as well as a review of the relevant literature.

2.1 Reaction Diffusion

Reaction diffusion is a field of science that has seen rapid innovations in the areas of image processing (Kuhnert et al., 1989) and chemical computing (Dittrich, 2004). Among the numerous computing approaches, it has emerged as an alternative that takes advantage of the intrinsic ability of chemically reactive circuits to process information similar to that of computers.

There are different reactions that produce oscillations, and the Belousov-Zhabotinsky (BZ) reaction is very popular. Others include the Briggs-Rauscher reaction (De Kepper and Epstein, 1982).

2.2 Belousov-Zhabotinsky Reaction

The Belousov-Zhabotinsky reaction 2.1 was discovered by Boris Belousov in 1951 and later further-studied and altered by Anatol Zhabotinsky in 1961. The reaction produces a chemical oscillation, which is a periodic change of the chemical concentration of two reactants. Belousov initially used malonic acid, potassium bromate, and cerium(IV) ions. Cerium was later changed to ferroin by Zhabotinsky in order to enhance the colour change of the reaction. Ferroin was later changed for ruthenium(II) ions (Toth and Taylor, 2006), which is light sensitive, is the most common catalyst used today. The reaction is done in a petri dish that is about 2mm deep. There are variations of it where all of the chemicals are not mixed together directly, but instead a catalyst is used to start the reaction. This is very useful as it allows for starting and stopping the reaction at will, which enables the creation of a chemical computer. A catalyst is a substance that increases the amount of excitement in a reaction, while not being consumed in the reaction itself. One very common approach to control the reaction is to use light to control the excitability, a method commonly used by Gorecki et al. (2003), where the catalyst in use is $\text{Ru}(\text{bpy})_3\text{SO}_4$.



Figure 2.1: Time-lapse of the Belousov-Zhabotinsky reaction in a petri dish done in the University of Stavanger

2.3 Chemical Computing

Chemical computing makes use of chemical reactions to perform operations. Turing (1952) is among the first to theoretically explore the field of Chemical Computing. His proposal was a model that could explain the creation of patterns in nature, such as the stripes on a zebra or the spots on a leopard. Since then the field has seen a lot of exploration. One of the pioneers there is Adamatzky et al. (2005), who has done a lot of work in the field. Adamatzky (2019) includes work on slime moulds that can solve mazes, both in real life and in simulations.

There is no activator directly present in the solution. This is the main idea behind the chemical computer, where the reaction is controlled by light. (Reddy et al., 1995)

2.4 Oregonator Model

The original Oregonator model uses 5 reactants: A, Y, X, B, and Z to form an oscillation. This project uses a more simplified and very popular model of the Oregonator, which makes use of only U and V as reactants and still accurately produces oscillations.

2.4.1 The Mathematics Behind the Oregonator Model

Field (2007) mathematical model illustrated by equation 2.1 and 2.2, which uses a set of differential equations developed to describe and mimic the behaviour of a real BZ reaction, by allowing for the calculation of the concentration of the reactants over time. The Oregonator model is used to simulate the Belousov-Zhabotinsky reaction, which is a chemical oscillator.

$$\frac{\partial u}{\partial t} = \frac{1}{\epsilon} \left[u - u^2 - (fv + \phi) \frac{u - q}{u + q} \right] + D_u \nabla^2 u \quad (2.1)$$

$$\frac{\partial v}{\partial t} = u - v \quad (2.2)$$

These equations form the basis of the simulation, allowing for the exploration of dynamic chemical systems through computational methods. The meaning of every part of the equation was discovered mostly through experimentation by me and not through research, but still serves as a great introduction to the model: u and v are the concentrations of the reactants. The reason there is two of them is to create a two-step process in order to make

an oscillation. $\frac{u-q}{u+q}$, shown in Figure 2.2, where q is set to a very small value is used to create a specific curve that controls how quickly the rate of the reaction ($fv + \phi$) changes u , depending on its own concentration. As there is less activator chemical (u), the rate of the reaction is sped up because the term is negative, as it becomes exactly q , it starts to slow down the concentration until u^2 starts getting too big and starts slowing it down. As u increases, v increases as well, and if it reaches a cell where u has a high concentration, it gets plugged into the equation and since the term $-(fv + \phi)\frac{u-q}{u+q}$ is negative, it rapidly shuts the value of u all the way to 0 and v follows, creating an oscillation. Strictly speaking, the equation can work without $\frac{u-q}{u+q}$, but this term is crucial for the proper operation of the oscillation as it allows for the proper formation of the tail of the waves. The reason for that is exactly the non-linearity of the term, which allows the edges of the wave that have a lower concentration to form outside of the bounds of the circuit because these parts of the circuit require extra help due to the negative impact of the illumination. Without that, the waves would still work just fine under no illumination, but as soon as they have to pass through a gate that is separated by light, they would die instantly and not be able to pass through. $D_u \nabla^2$ is the concentration of the neighbouring cells that diffuse into the current cell, which adds dimensionality to the process because now the equation starts operating in 2D and every cell computes its own concentration based on the concentration of the cells around it. ϕ is external illumination that moulds the circuit where the reaction takes place by being set to either ϕ_{active} or ϕ_{passive} , active meaning the reaction is allowed to happen, or passive where it's very difficult for u to reach a critical concentration to start growing before it gets shut down by the second term of the reaction. The reason that u^2 does not decrease the reaction in the beginning is that the values of the reactants is very small and being squared makes them even smaller, but as they grow, the decrease becomes more meaningful. All of these parameters are set to specific values that are commonly used in literature in order to strike a difficult balance where the oscillation works in a way where chemical circuits are possible.

There are two main uses of the Oregonator model when it comes to parameters that change the behaviour of the reaction, the first one creates waves that do not expand. They travel without changing their shape, and the second one creates waves that expand, which is the one used by this project. Both ways have been shown to be able to create a Turing pattern, where the chemical circuits are vastly different, making use of the different properties of each model use-case. Stone et al. (2008) recreates an AND gate (Coincidence Detector) using the non-expanding wave method and the circuit is longer and more tunnel based. Most circuits in the expanding wave model are smaller as they rely on the intrinsic properties of the waves to hold more information in their shape, which is not possible in the non-expanding wave model where the waves are simpler are just travel along the non-illuminated gel material

2.5 Motivation

Although there is much potential there, most research focusses on building circuits in a simulation, such as Stovold (2019), versus in real life, such as Gorecki et al. (2003). It is unclear whether exactly how the simulation maps to real life in terms of size and environmental factors that are likely to impact it. This is the reason for the focus of this project to be in between the real-life reactions and the simulations, looking at the impact of the imperfections of the environment on the computation.

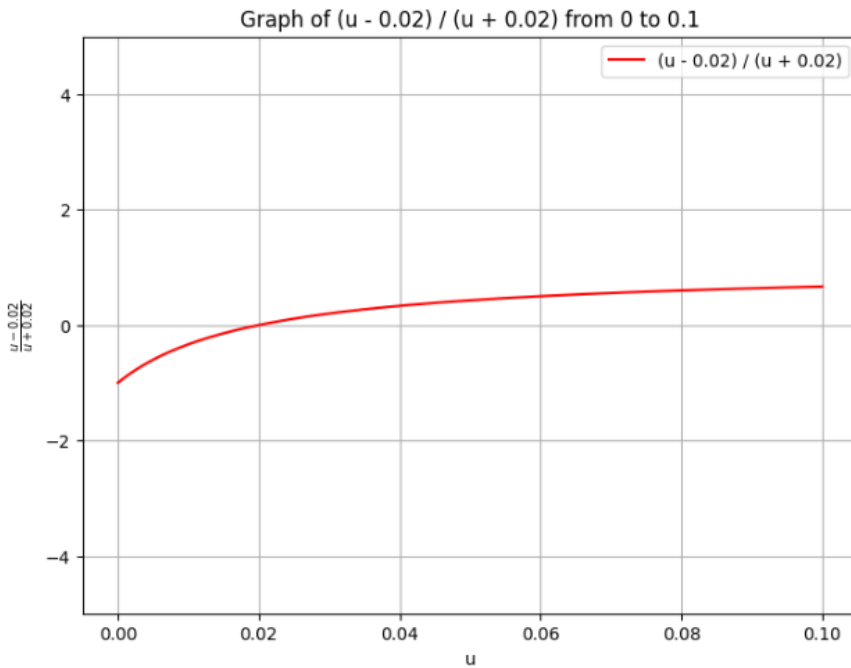


Figure 2.2: Graphical representation of the function $\frac{u-q}{u+q}$ showing how it influences the reaction rate in the Oregonator model

2.6 Goals & Objectives

- (1) Find if there is a mapping between the size of the computer in the simulation and the size of the computer in real life.
- (2) Explore how changes in light affect chemical computers
- (3) Recreate Stovold and O'Keefe (2017) in real life.
- (4) Investigate the effects of temperature variations on the computer.

3 Design & Implementation

The project experimented with Flutter for the initial simulation due to the benefits of pixel-level control and fast prototyping (see Figure A.1 for a preview of the first successful waves). However, the rendering was too slow for large chemical circuits, so the GPU was needed, for which, as of March 2024 Flutter still has no official support. A custom version of the newest engine was tested to expose experimental GPU APIs as detailed in flutter.dev/go/impeller-dart. That did not work, so the Metal library was used to compute the simulation on the GPU. The Metal library is a low-level, high-performance API for the GPU, and it was chosen for its ability to run on Apple devices, which are widely used in the scientific community, the execution graph for the simulation is illustrated in Figure 3.1. The implementation is done using two buffers and two CPU threads. While the compute thread is computing the next state of the simulation by sending commands to the GPU, the render thread is displaying the current state of the simulation on the screen. The CPU has no knowledge of the state of the simulation and the assets used stay solely on the GPU, both during computation and during rendering. This allows for very high performance that is possible only because of the fact that there is no copying of data between the CPU and the GPU aside from simple buffers used for communication.

Conducting measurements was implemented using a sampling shader, which runs on the GPU, it is given a coordinate and returns information back to the CPU. This is desyncronised from the computation of the simulation because it does not run on the compute thread. Another more efficient and accurate way to measure is to add the measurement buffers directly to the compute shader. That would allow for the measurement to happen at the same time and could also track the simulation time steps, which is something that is not easy with the current implementation.

The mathematical principles in the Oregonator model are described in section 2.4.1. The parameters for the simulation are listed under table 3.1. They are standard values widely used in the literature that experiments with the Oregonator model. What each of them does is described in Chapter 1.

Parameter	Value
ϵ	0.0243
f	1.4
ϕ_{active}	0.054
ϕ_{passive}	0.0975
q	0.002
D_u	0.45
Δt	0.001
Δx	0.25

Table 3.1: Simulation parameters with their respective values.

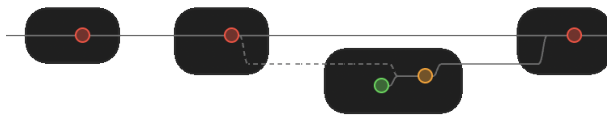


Figure 3.1: The Metal Dependency Pipeline consists of a Compute Command Encoder (represented by red circles) and a Render Command Encoder (depicted by yellow circles). The Compute Command Encoder is run multiple times, performing as many calculations as possible. Simultaneously, the Render Command Encoder operates periodically to render the computed results. These two encoders work in parallel, with the Render Command Encoder producing output every time it gets a chance, while the Compute Command Encoder continuously performs computations most of the time.

4 Results

This chapter aims to explore the operational boundaries of the chemical components in a Petri dish environment, focusing on the size limitations of the coincidence detector and the light sensitivity of a chemical diode. A coincidence detector is crucial in the design of chemical circuits because it allows for an implementation of AND gates, which are important for computing. This detector is illustrated in Figure 4.3 and it works by having two waves come together from left and right and if they meet, they form a new wave that passes through the detector at the bottom.

The main objectives of the experiments are to find out the bounds and limitations of different chemical components in order to determine the feasibility of using them in a real-world environment.

4.1 Creating a Coincidence Detector In Simulation

The project aims to explore the mapping between the size of the computer in the simulation and the size of the computer in real life according to Goal 1 in Section 2.6. This cannot happen if there is no computer to begin with, so the first step is to create a computer in the simulation. A whole computer would be cumbersome to create, so we start with creating a Coincidance Detector, also known as an AND gate, as it is one of the simplest computations that can be created in chemistry

Developing the AND gate posed a significant challenge as it is highly dependent on specific geometric configurations for proper operation. While it is acknowledged that such a coincidence detector is feasible, the focus of our investigation is on the stability of such simulations in response to environmental changes and the practicality of implementing them in a real environment. Although we acknowledge that building this in a simulation is possible, the focus of this paper is to determine the stability of the simulation in response to environmental changes and the practicality of implementing them in a real environment.

4.1.1 Unsuccessful Detector

In our investigation, we focus on three controllable variables:

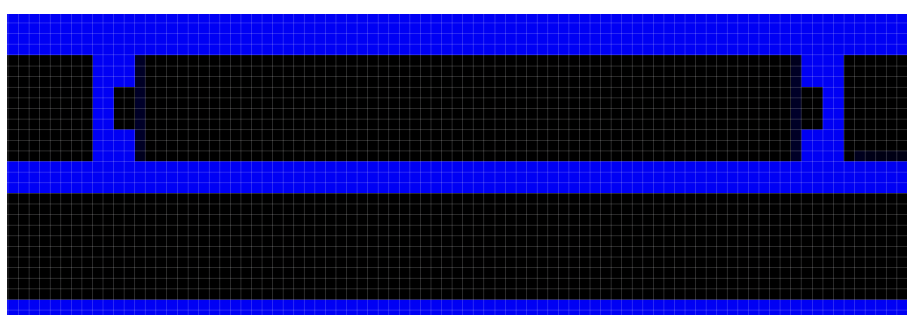


Figure 4.1: Initial Coincidence Detector Configuration

4 Results

Width	Gap=1px	Gap=2px	Gap=3px	Gap=4px
w=1px	NP	NP	NP	NP
w=2px	NP	NP	NP	NP
w=3px	AP	NP	NP	NP
w=4px	AP	AP	NP	NP
w=5px	AP	AP	NP	NP
w=6px	AP	AP	NP	NP
w=7px	AP	AP	NP	NP
w=8px	AP	AP	NP	NP
w=9px	AP	AP	NP	NP
w=11px	AP	AP	NP	NP
w=12px	AP	AP	NP	NP
w=13px	AP	AP	NP	NP

Table 4.1: Results of the experiment showing the relationship between conductor width and gap size.

- the width of the conductor
- its length before the gap.

The detector configuration is shown in Figure 4.1. The primary question we seek to answer is how the width of the conductor influences the functionality of the gates. Specifically, our experiment aims to identify an optimal conductor width that enables the "if" gate to function correctly. This gate's operation relies on two conductors positioned closely, requiring a precise amount of force to facilitate signal transmission from one to the other. This force is generated by the collision of two waves. However, current configurations fail due to the conductors being excessively proximate.

For the purposes of this experiment, we define three outcomes based on the interaction between the waves and the conductors: - Always pass (AP): The signal always passes through the gap. - Never pass (NP): The signal never passes through the gap. - Collision pass (CP): The signal passes through the gap only upon collision of waves.

The CP outcome is of particular interest as it represents the desired state for computational functionality.

Initial tests did not yield CP outcomes, suggesting a potential discrepancy in the values of ϕ_{active} versus ϕ_{passive} . Adjusting ϕ_{active} to a more aggressive value of 0.035f resulted in CP outcomes for every gap of 3px, marking a significant deviation from the default value of 0.054 proposed in prior literature. This finding prompts further investigation into the range of values between 0.035 and 0.054 to identify a flexible operational window.

A successful configuration identified involves a long charge, a gap of 3px, and a ϕ_{active} value of 0.035. Further exploration is required to determine a viable configuration for a gap of 2px.

Additionally, our observations reveal notable differences in wave behavior depending on orientation; specifically, vertical wave propagation exhibits distinct properties compared to horizontal propagation. A particularly intriguing observation is that waves originating off-center tend to accelerate asymmetrically, favoring one direction over the other, and resulting in a higher likelihood of collision.

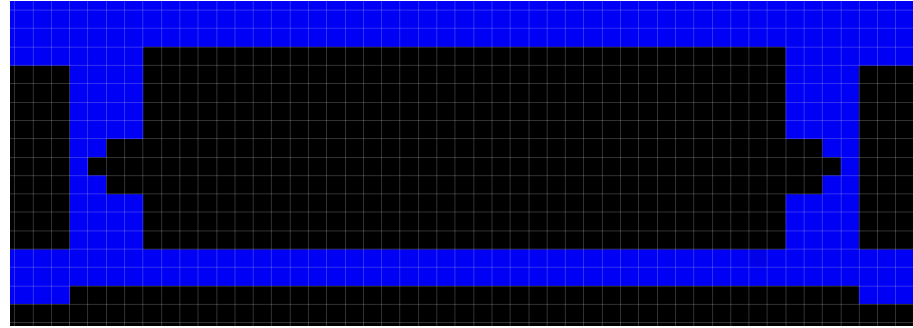


Figure 4.2: First Successful Coincidence Detector

4.1.2 Successful Detector

Section 4.1.1 led to the conclusion that there must be more parameters in play that prevent the detector from functioning, and it was later found that the height of the diode pin on the active medium of the coincidence detector. Following this, it was discovered that by setting the pins higher or lower, we change from where the wave approaches the detector medium, allowing for a finer adjustment of the operation. This created the first successful detector, seen in Figure 4.2.

Normally the wave also depends on where it is coming from, but we can ignore that in our case because we are using diodes at entry of the detector medium. Diodes add a new entry point for the incoming wave, so the incoming direction does not really matter.

There is still a small problem with this design where if two waves meet around the centre, none of them gets enough momentum to develop fully and they do not have enough concentration to diffuse into the result substrate, this can be solved by increasing the length of the detector medium to allow for both waves to form, so later designs have a longer detector medium, like in Figure 4.3

The length of the coincidence detector depends on two factors:

1. The minimum distance apart they need to be from each other while still allowing for the waves to form inside the detector.
2. The minimum distance apart they have to be, so that the centre is still usable for collision.

This will be used in Section 4.2 to compare it with a real chemical AND gate to establish a mapping.

4.2 Mapping the Simulation Size to Real Life

In order to understand how real light affects the chemical circuit, what needs to be established is the resolution of the circuit in real life and how it relates to the size of the detector. Gorecki et al. (2003) have recreated the circuit in a Petri dish, so we can use the size of the circuit in the Petri dish to map it to the size of the circuit in the simulation. The goal here is to find a way to measure the size of the coincidence detector in real life, for which there is currently no data. The size of the coincidence detector is crucial for the design of the Petri dish, as it determines the minimum size of the Petri dish required to accommodate the detector.

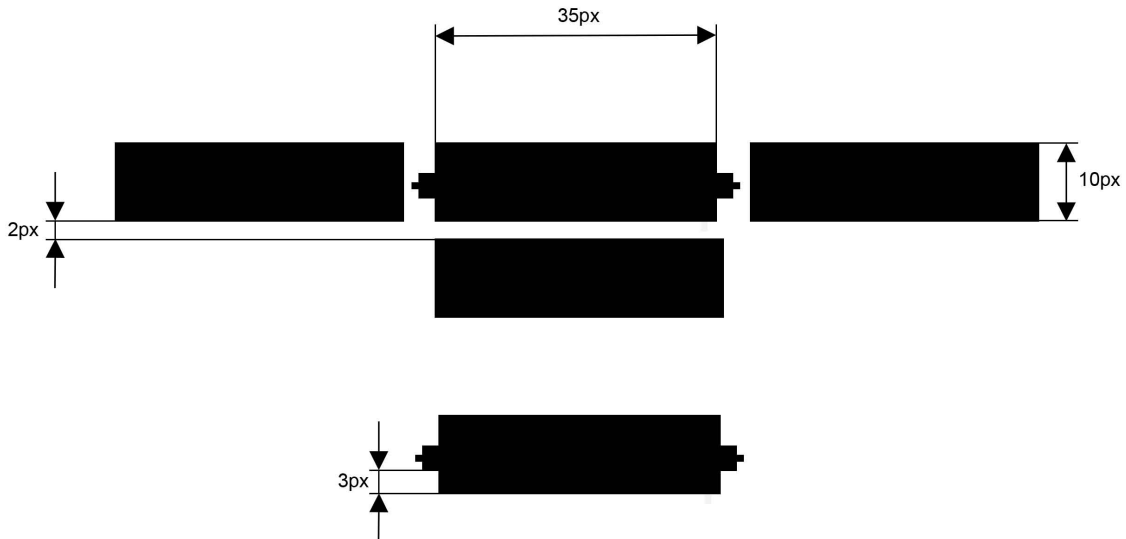


Figure 4.3: First working AND gate

In order to measure that, the coincidence detector had to be designed first and that is covered in Appendix 4.1, the final component is illustrated in Figure 4.3.

The design of the detector (Fig. 4.3) implies that there is no max size for the length of the coincidence medium in the detector circuit as the waves have a width equal to the width of the coincidence channel.

Assumption

The size of the Petri dish is **assumed** to be unsubstantially larger than the size of the chemical circuit inside of it. Continuing from both sizes are referred to interchangeably.

A significant milestone in the practical application of chemical computing was achieved through the real-life implementation of an AND gate using the Belousov-Zhabotinsky (BZ) reaction. This implementation, detailed by Gorecki et al. (2003) and shown in Figure 4.4, serves as a cornerstone example of how chemical reactions can be harnessed for computational purposes.

Now, this is just a simulation we are doing, so to get the mapping for a real Petri dish, we can use the dimentions of the gate in a Petri dish. In Gorecki et al. (2003), the exact dimensions in mm of the collision detector, signal channel of 10cm, and a membrane filter of 2.5cm inside of the Petri dish are specified. These dimensions can be used to map it to the one in our simulation.

Given the following mapping from real life measurements to simulation pixels:

- Stripe width: 2 mm = 10 px
- Channel gap: 0.4 mm = 2 px

We can establish a scaling factor for the conversion from millimeters to pixels. For the stripe width:

$$\text{Scaling factor} = \frac{10 \text{ px}}{2 \text{ mm}} = 5 \text{ px/mm}$$

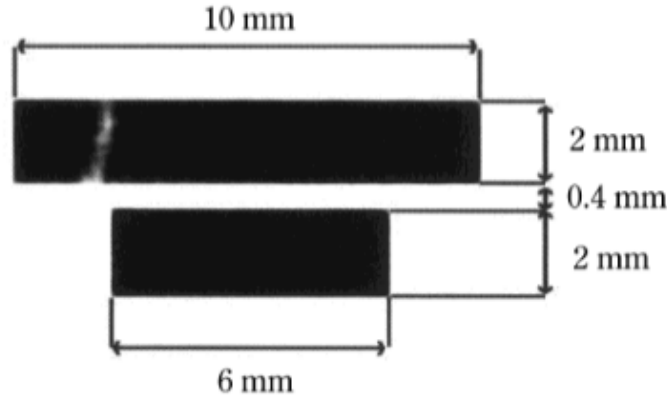


Figure 4.4: Real-life AND gate using BZ reaction (Gorecki et al., 2003)

For the channel gap:

$$\text{Scaling factor} = \frac{2 \text{ px}}{0.4 \text{ mm}} = \frac{2 \text{ px}}{\frac{2}{5} \text{ mm}} = 5 \text{ px/mm}$$

Thus, both measurements confirm the same scaling factor. Using this consistent scaling factor, we can convert any measurement from millimeters to pixels.

Using this scaling factor, we can convert any measurement from millimeters to pixels. For a dimension of $10 \text{ mm} \times 4.4 \text{ mm}$, the conversion would be:

$$\text{Width in pixels} = 10 \text{ mm} \times 5 \text{ px/mm} = 50 \text{ px}$$

$$\text{Height in pixels} = 4.4 \text{ mm} \times 5 \text{ px/mm} = 22 \text{ px}$$

Thus, a real-life size of $10 \text{ mm} \times 4.4 \text{ mm}$ would map to a size of $50 \text{ px} \times 22 \text{ px}$ in the simulation. More importantly, the simulation uses details as small as 1px^2 , which would amount to $\frac{1}{5}\text{mm}^2$ in real life, which would be infeasible because details smaller than 1mm^2 are difficult to control accurately. This means we would need to scale the simulation up in order to have details easier to control. However, as we scale it up, the surface area of the Petri dish becomes larger and the angle of incidence of the light becomes more significant, which is a problem we will explore later on in section 4.4. The reason there is a section before that is because _____

help

4.3 Finding ϕ_{\min} and ϕ_{\max} for a Chemical Diode

As mentioned in equation 2.1, ϕ is external illumination that creates the chemical circuit. It sets the value of ϕ to either ϕ_{active} or ϕ_{passive} . ϕ values control the lighting conditions of the chemical circuit. Active regions are where it is dark/unilluminated and passive regions are where there is light/illumination. The reason behind the need to measure the ϕ values for a Chemical Diode stems from the fact that a chemical diode is less sensitive to changes in ϕ values than other chemical components. This means that the diode can still operate even outside the values for ϕ established in literature. In order to see where chemical computers break, we need to measure each component and see where it breaks. The operational range for a whole computer is the intersection of the operational ranges of every component, which is equal to that of the most sensitive performing component. Here

ϕ_{passive} is measured at different values because that is the value controlling the illuminated area, which makes the circuit there “passive”. This simulates less illumination of light at the diode, altering its behaviour.

4.3.1 Measuring ϕ_{\min} , ϕ_{\max}

During the evaluation of ϕ_{\min} , ϕ_{\max} , the diode had to be tested from numerous directions to determine the minimum and maximum values of ϕ_{passive} where it still functions correctly as a diode, which means that it passes waves from right to left, but never from left to right. As we approach the limits, new cases start appearing where the wave becomes able to pass through from a very specific angle that changes as we change the phi value, making it impossible to automatically test, so manual testing was needed to verify if the diode works in every single use case for the limit phi values. Also, the minimum and maximum values start to highly depend on the testing conditions, and whether the diode works or not starts to depend on how you are using it; for example, do you start a wave right at the diode? If not, what is the minimum distance the diode has to work for? This greatly changes the minimum and maximum phi values.

Measurement Methodology

The measurement was done by starting a wave at a distance from the diode and measuring if it passes through the diode. It's done from both directions. Tested from multiple angles and distances and qualitatively assessed if it still performs as a diode under every single case. The investigation is trying to establish ϕ_{\min} and ϕ_{\max} for the diode, which are the operational boundaries for the ϕ_{passive} values that the diode can tolerate, which represent the less than ideal lighting conditions are trying to explore. We know that the diode operates mostly at $\phi_{\text{passive}=\phi_{\text{litrature}}} = 0.0975$. We start from this value and start going in both directions, increasing and decreasing the value of ϕ_{passive} and measuring if the diode still works. $\phi_{\text{current}} = \phi_{\text{litrature}} = 0.0975$

Algorithm 1 outlines the process of finding the boundaries of ϕ_{passive} for the diode. It is run twice, once with $\text{step}=0.05$ and once with $\text{step}=-0.05$ to go in the other direction.

Results

Results of measurement:

- $\phi_{\max} = 0.106127$
- $\phi_{\min} = 0.09555$

That is, as long as $\phi_{\min} < \phi_{\text{passive}} < \phi_{\max}$, then the diode will function as expected, even though the propagation time would still be affected (as seen in Figure 4.6), causing synchronisation problems in larger circuits.

4.3.2 Propagation Time Variation of the Diode Under Different Lighting Conditions

The reason we are looking at propagation time variation is because if that changes in response to the lighting conditions, then the diode will behave as expected, but larger

Algorithm 1 Detailed ϕ Exploration Algorithm. It works by starting from $\phi_{\text{literature}}$ and searching for the last value where the diode still works. The function TestDiode returns true if the diode works and false if it does not. This is done manually by performing comprehensive tests on the diode from both directions. It should let the wave through from right to left, but never from left to right. This shall be true for all angles and distances. The whole algorithm is run manually and is written out here just for illustrative purposes.

```

1:  $\phi_{\text{current}} \leftarrow \phi_{\text{literature}}$ 
2:  $precision \leftarrow 0.5$                                 ▷ Starting precision
3:  $step \leftarrow 0.05$                                  ▷ Initial step size
4: while  $precision \geq 0.0001$  do                  ▷ Continue until precision is fine enough
5:    $found \leftarrow \text{false}$ 
6:   while not  $found$  do
7:     if TestDiode( $\phi_{\text{current}} + step$ ) then
8:        $\phi_{\text{current}} \leftarrow \phi_{\text{current}} + step$ 
9:     else if TestDiode( $\phi_{\text{current}} - step$ ) then
10:     $\phi_{\text{current}} \leftarrow \phi_{\text{current}} - step$ 
11:   else
12:      $found \leftarrow \text{true}$ 
13:   end if
14: end while
15:  $precision \leftarrow precision/10$                       ▷ Increase precision
16:  $step \leftarrow 0.5 * precision$                          ▷ Adjust step size based on new precision
17: end while
18:  $\phi_{\text{functional}} \leftarrow \phi_{\text{current}}$ 

```

4 Results

circuits that synchronise with the output of that diode and other chemical components will be affected by this change and might not work as expected.

Methodology

The way the experiment was set up was that a diode was set up in Figure 4.5 where a wave was launched 25 px from the diode to allow it to pass through the diode and reach a small white flag where the wave is expected and the experiments are evaluated. A step in the diagram means one simulation pass. The parameters of the experiment were the following:

- Number of ϕ_{passive} values: 30, of which only 19 succeeded, the remaining 11 could not pass through the diode due to the parameter being too out of range.
- Interval size: 0.0013448276
- Number of runs per ϕ_{passive} values: 7
- ϕ_{start} : 0.08066608
- ϕ_{end} : 0.121010914, never reached because once a wave passes through the diode, the concentration no longer reaches zero fully and that leaves a very small amount of inhibitor at the diode and due to the borderline value of ϕ_{passive} the next waves never manage to penetrate to get measured, so the highest measured value for ϕ_{passive} is 0.10487298
- Wave start: 39px before diode, which was observed to be enough to allow for the proper formation of the wave such that it can pass through the diode.
- Wave measure: 31px after diode, which was far away enough to measure a fully formed wave, provided that one passed through the diode.
- dt : 0.001, also serves as a reference point for the amount of steps.
- Measurement interval: about every 5 steps, depending on the GPU frame rendering schedule

It is possible to run the experiment much more accurately, eliminating the need for multiple runs for the same ϕ_{passive} value we measured at every step and did not simulate another step in the simulation until the measurement was complete. However, that would drastically slow down the experiment, making it run for hours instead of minutes. For the purposes of merely showing that the propagation changes along with the slope, it was enough accuracy, so the faster and more inaccurate solution was chosen.

So, the following limitation were found while working with the simulation. Due to the act that in metal sampling is a rendering operation, it cannot be done during the computation of the simulation. That means that I would have to synchronise it to run with rendering speed, but that would make the simulation too slow to run many experiments. It uses the step speed of the simulation, 1 frame = about 150 steps in the simulation. This is still accurate enough. I ran at $dt = 0.001$. To get better results the computation was run at $dt = 0.001$ was done every 300 microseconds. Additional values were added in between ϕ_{min} and ϕ_{max} where the curve started to change, and the results can be seen in Figure 4.7.

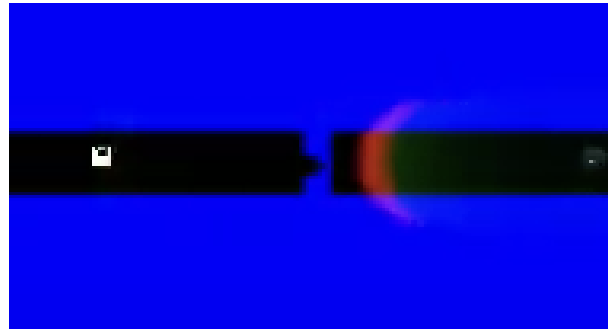


Figure 4.5: Diode Experiment

4.3.3 Results

The results of the experiment can be seen in Figure 4.6. The propagation time decreases as there is less light, indicated by the decrease in the value of ϕ_{passive} and the reverse. This is to be expected, as a lower value brings it closer to ϕ_{active} (darkness), and illumination is an inhibitor. The reason the circuit has a higher tolerance to less light, compared to more light, is because the diode is much more resistant in the reverse direction as the wave has to go through a reverse triangle, which is specifically made to stop the propagation of waves. The diode also has a high tolerance to ϕ_{passive} increasing due to an additional spike added to the diode, which helps weaves to cross the gap easier, even when there is more light. The reason for $\phi_{\text{max}} < \phi_{\text{end}}$, meaning the diode was still letting the wave through left to right and not right to left at ϕ_{end} , but it was not at other angles when tested, so the experiment measured propagation time, but the diode was only partially functional at these values

4.4 Estimating The Light Source's Position

Identifying the minimal operational conditions for the AND gate in real life involves examining light intensity, angle of incidence, and the effect of the thickness of the beam of light on the BZ reaction.

Some circuits can be influenced by temperature, such as Yamada et al. (2022), which uses a more complex model of the oregonator. .

Shining light on the BZ surface: (Barry et al., 1979) The catalyst in these reactions is light, using light we can modulate the speed using Φ . A light bulb is shined over the Petri dish (fig. 4.9a)

Given multiple light sources, the total illumination I_{total} at a point on a surface is the sum of the illuminations from each individual light source (fig. 4.9b). The illumination I_i from a single source at a given point is given by the inverse square law, adjusted for the angle of incidence θ_i :

$$I_{\text{total}} = \sum_{i=1}^n \frac{P_i}{4\pi r_i^2} \cdot \cos(\theta_i)$$

where P_i is the power of the i -th light source, r_i is the distance from the i -th light source to the point, and θ_i is the angle between the direction of the i -th light ray and the normal to the surface. The cosine term $\cos(\theta_i)$ accounts for the angle of incidence, with the intensity contribution from the light source decreasing as the angle increases.

is it the
same reac-
tion

4 Results

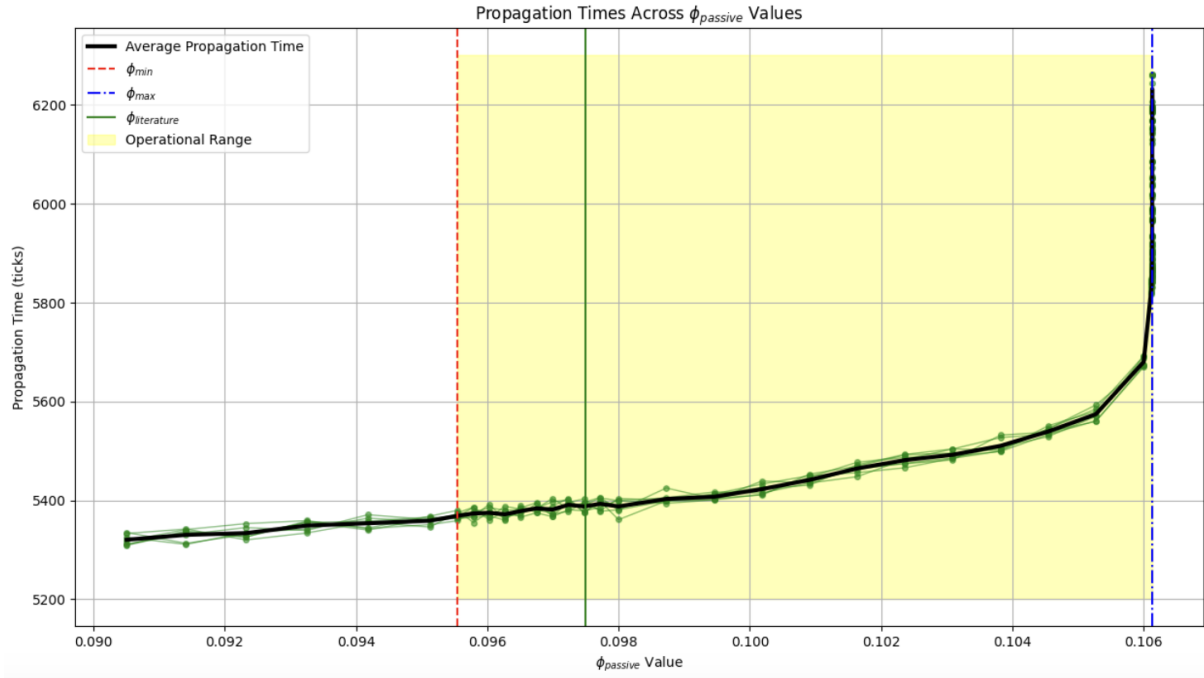


Figure 4.6: Propagation times for various ϕ_{passive} values within the limits of ϕ_{\min} and ϕ_{\max} , illustrating the experimental outcomes of testing a diode in a Belousov-Zhabotinsky reaction. Each point represents a propagation time measurement for a given ϕ_{passive} , with the average propagation time across measurements shown by a thicker black line. The shaded area between ϕ_{\min} (red dashed line) and ϕ_{\max} (blue dashed line) highlights the range where the diode works correctly, with the ϕ used commonly in literature marked by a solid green line.

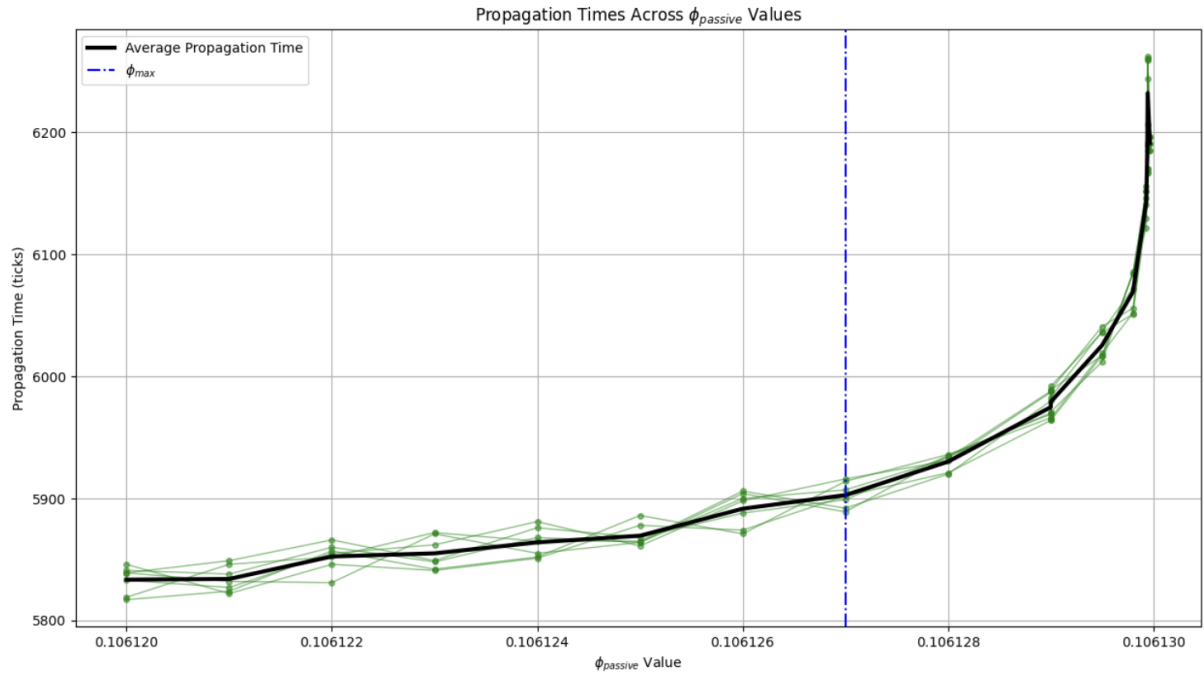


Figure 4.7: Propagation times around the value of ϕ_{\max} . The range of ϕ is $\phi_{\max} - 7 \times 10^{-6} \leq \phi \leq \phi_{\max} + 3 \times 10^{-6}$

4 Results

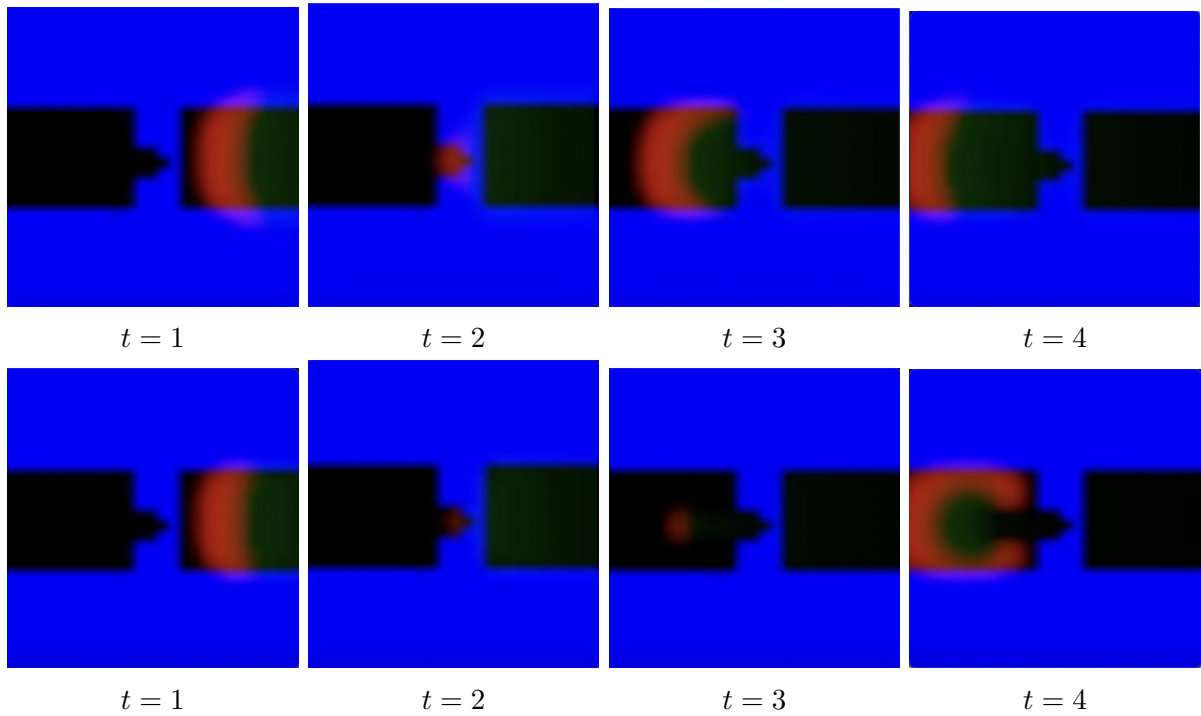


Figure 4.8: Comparison of two waves passing through a diode. Above $\phi_{\text{passive}} = \phi_{\text{literature}}$, below $\phi_{\text{passive}} = \phi_{\max}$. Both have different propagation speeds, so they have been equalised for the purpose of comparing their interaction with the diode side by side. The second wave takes substantially more time to form and is about 700 time steps slower as seen in Figure 4.7, which is quite a lot in such simulations.

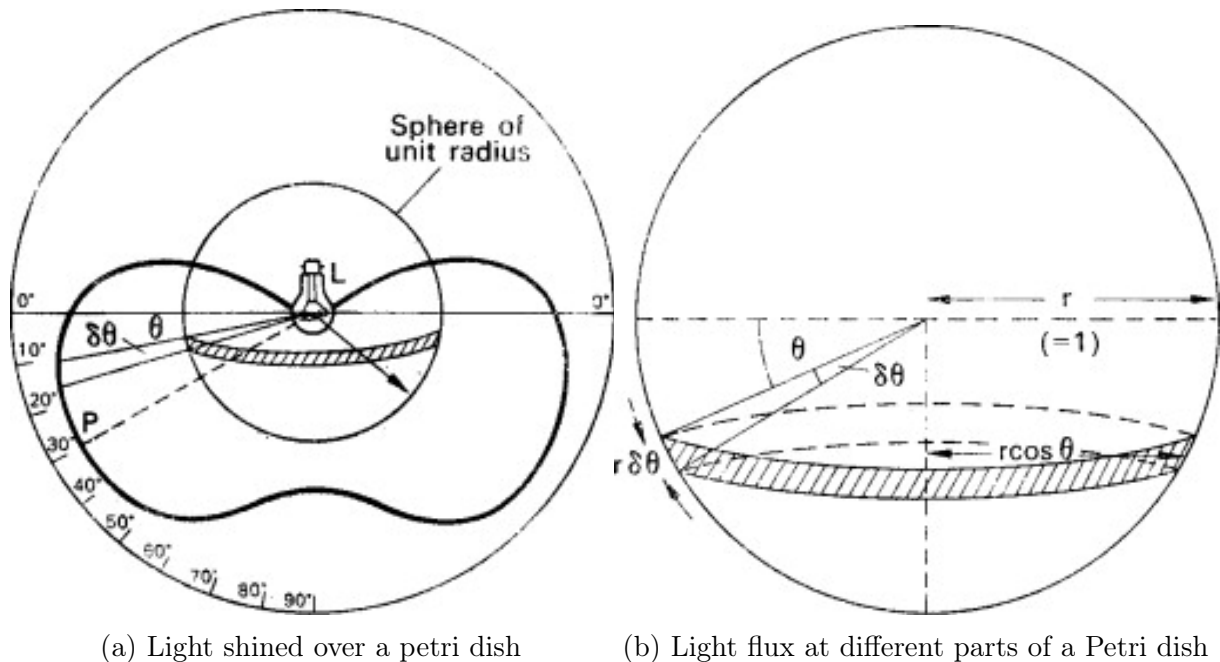


Figure 4.9: Visualization of light interaction with a Petri dish (Edwards, 1970).

4 Results

This means that now we can use that in the simulation to simulate the imperfections of light sources.

Most uses a single light bulb to illuminate the Petri dish as the Petri dish is small.

It is very important to calculate how far away the light source is from the Petri dish in order to make useful light calculations later on. This is because if the light source is very far away, the angle of incidence θ is very close to 90° , so the effect of the angle is insignificant.

In real experiments, the chemical reaction that occurs on the gel surface is sensitive to light due to the specific catalyst used ($\text{Ru}(\text{bpy})_3\text{SO}_4$). However, to observe and record the process, they need to use light to illuminate the gel, so that the camera can capture images. The experiment design, including time-varying intervals of different light intensities, allows them to balance between controlling the reaction and capturing the activity on the gel. Toth et al. (2009)

They all project a single light bulb and then use a mask to have the shape they want projected, such that light does not kill off the reaction and there is light everywhere else. This is important to show how imperfections can affect the simulation . Gorecki et al. (2003) An experimental setup for observing pulses in a photosensitive BZ reaction, as detailed in the work by Gorecki et al., is illustrated in the following Figure 4.10. This setup is crucial for understanding the dynamics of light-sensitive chemical reactions and their applications in computational models.

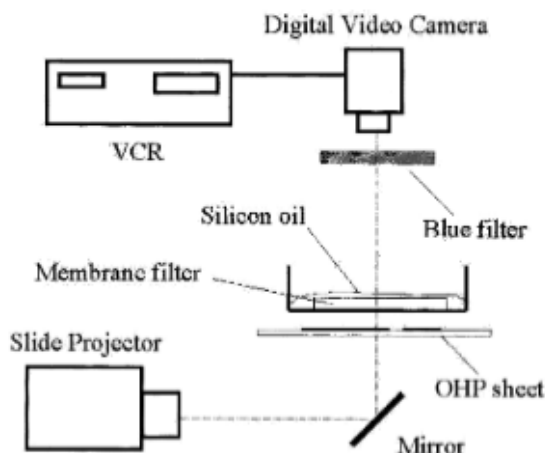


Figure 4.10: Experimental setup for observing pulses in a photosensitive BZ reaction (Gorecki et al., 2003).

(Cui, 2004, 71) contains a similar setup and goes into more detail how they project the pattern onto the gel. The book goes into more detail helpful for understanding the real-life environment where the waves propagate. One interesting observation is that the observation angle seems to change where we see the wave, which might be relevant for measuring the size of the waves, however this is not explored in this project.

Assumption

Unfortunately, Gorecki et al. (2003) do not specify how far away the light bulb projector is, which is used to illuminate the Petri dish, but we can assume the projector is far away, such that the angle of light projection is very close to 90°, making the effect of the angle insignificant.

We can still simulate that in our simulation to see what effect it would have if it were close to the medium; for larger circuits, this effect would be visible. Given a normal setup, what would be the maximum size of the Petri dish in a simulation before the effects of the light angle start to impact the simulation.

The distance between the active channel and the signal bar is 0.4 mm, which corresponds to exactly 2px in the simulation.

Both stripes are 2 mm wide, the signal channel is 10 mm long, and the detector part is 6 mm long. The gap between the signal and the detector channels is 0.4 mm. The light intensity was selected so that the non-illuminated parts of the membrane were excitable, whereas the excitations died in the illuminated areas. In the experiment, the light intensity was set at I = 24 kLx as determined by a light metre (ASONE LM-332), and the temperature was 295 ± 1 K (Gorecki et al., 2003).

From the provided information in the paper and the datasheet for the JCD100V-300W halogen bulb, we have the following data:

- Luminous flux (Φ) as specified in the datasheet = 6600 lm (Fujilamp, 2024)
- Light intensity (I) at the Petri dish = 24,000 lux

Originally, we calculated the luminous flux using the estimated luminous efficacy of $17 \frac{\text{lm}}{\text{W}}$ and the power of the bulb (P) as 300 W, which gave us:

$$\Phi_{\text{estimated}} = \text{Power of bulb} \times \text{Luminous efficacy} = 300 \text{ W} \times 17 \frac{\text{lm}}{\text{W}} = 5100 \text{ lm}$$

However, this was an approximation. The datasheet for the bulb specifies a luminous flux of 6600 lm, which suggests that our assumption for the luminous efficacy was incorrect.

Using the inverse square law, which relates the light intensity (I) to the distance (r) from the light source, we have:

$$I = \frac{\Phi}{4\pi r^2}$$

Solving for the distance (r) with the correct luminous flux, we get:

$$r = \sqrt{\frac{\Phi}{4\pi I}}$$

Substituting the values from the datasheet and the light intensity measurement, we find:

$$r = \sqrt{\frac{6600 \text{ lm}}{4\pi \times 24,000 \text{ lux}}}$$

$$r \approx 0.148 \text{ metres}$$

Thus, the corrected distance from the light source to the Petri dish, using the accurate luminous flux from the datasheet, is approximately 0.148 metres or 14.8 centimetres. This

4 Results

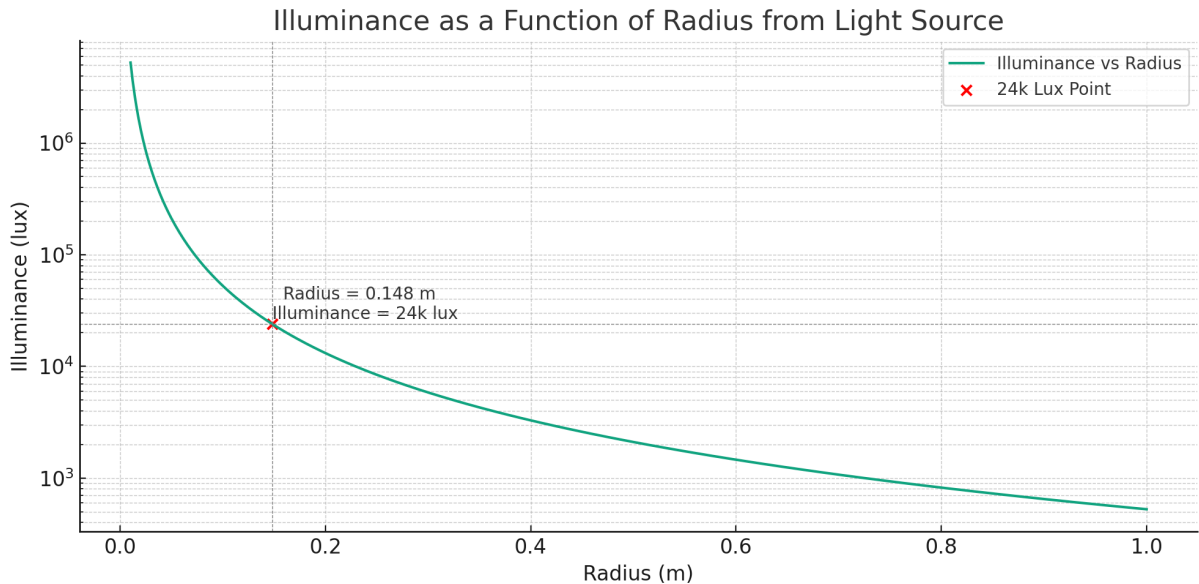


Figure 4.11: Radius Illumination Graph

distance is crucial, as it suggests that the light intensity measurement of 24 kLux is likely taken close to the Petri dish where the biological samples are studied, rather than at an arbitrary point close to the light source.

In figure 4.11 it is shown how the radius impacts the intensity at the light. Given the luminous flux Φ of the JCD100V-300W bulb as 6600 lumens, we can calculate the illuminance I at various distances from the light source. The illuminance is given by the formula:

$$I = \frac{\Phi}{4\pi d^2}$$

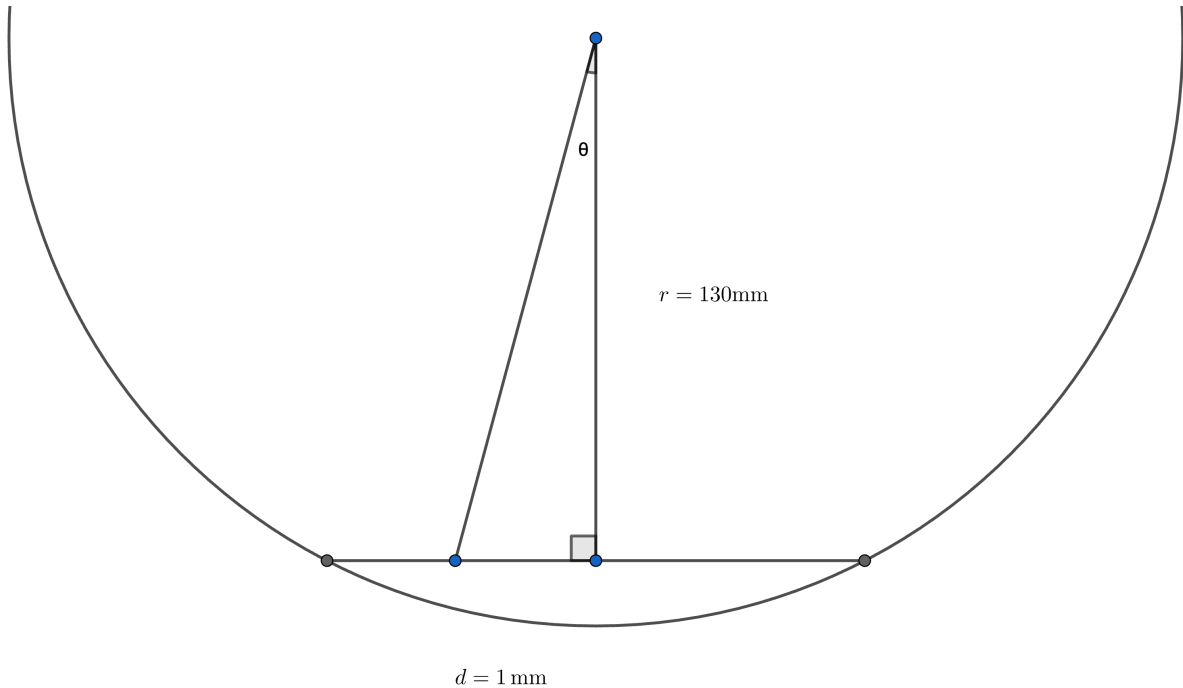
where d is the distance from the light source in meters.

For distances of 10 cm, 12 cm, 18 cm, and 20 cm, the illuminance values calculated are:

- At 10 cm: $I \approx 52521$ lux
- At 12 cm: $I \approx 36473$ lux
- At 18 cm: $I \approx 16210$ lux
- At 20 cm: $I \approx 13130$ lux

These values illustrate a significant change in illumination as the radius increases, indicating that the radius is a crucial factor in determining the intensity of light received at a point.

Concluding from these calculations, it is likely that the measurement of 24 kLux was made relatively close to the Petri dish. This is because the light intensity of 24 kLux is a practical measure for the conditions under which biological samples are typically studied. Measuring illuminance right next to the light source would yield an impractically high value, which is not as useful for experimental purposes. Hence, the measurement taken is more likely to be representative of the actual working conditions near the Petri dish.


 Figure 4.12: Illustration of finding the angle θ

4.5 Estimating The Maximum Petri Dish Size for a Chemical Diode (Gorecki et al., 2003)

Next thing is to add the imperfection in the simulation with only an AND gate. To do that, I need to come up with a formula about plugging in a pixel and getting out the illumination percentage. The percentage is basically the $\cos \theta$ as it is 0 when the angle is 90° . let's assume a parallel light source is max intensity and an angle of 0 is no intensity at all, so in the formula we would plug in $\phi = 0.054$ for when it's active and $\phi = 0.0975$ when it's passive. Active means no light, passive means a lot of light, so when the light source becomes weak at a point, that would mean that ϕ becomes more active. let's come up with a formula in mm that tells us when we move 1mm from the center of the petri dish where the light is most intense, what angle is that. That should be pretty simple, we have a right triangle,

We have to find the angle every time when we move x mm from the center of the petri dish.

To calculate the angle θ for any given radial distance r_c from the center of the Petri dish, we convert the pixel distance p to millimeters using the scaling factor s (in px/mm):

$$r_c = p \times s$$

The angle θ is then found using the arctangent function with respect to the height h of the light source above the center of the Petri dish:

$$\theta = \arctan\left(\frac{r_c}{h}\right)$$

The percentage of illumination I_p at this radial distance is given by the cosine of θ :

$$I_p = \cos(\theta)$$

4 Results

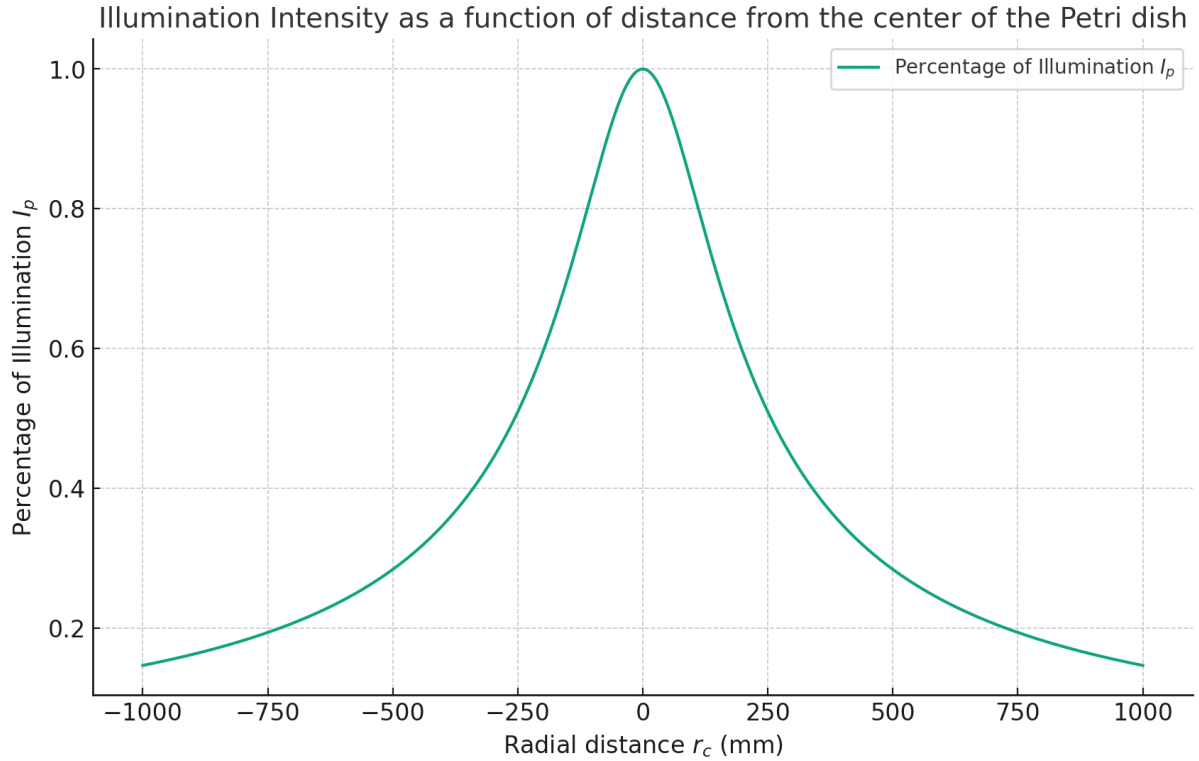


Figure 4.13: The graph represents the percentage of illumination I_p as a function of the radial distance r_c from the center of the Petri dish. The illumination percentage is calculated using the equation: $I_p = \frac{1}{\sqrt{1 + (\frac{r_c}{h})^2}}$ where r_c is the radial distance from the center of the Petri dish in millimeters, and h is the height of the light source above the center of the Petri dish, which is 148 mm. The graph extends from $r_c = -1000$ mm to $r_c = 1000$ mm to illustrate the symmetrical decrease in illumination intensity on both sides of the center point.

Since $\cos(\arctan(x))$ simplifies, we can express I_p directly as:

$$I_p = \frac{1}{\sqrt{1 + \left(\frac{r_c}{h}\right)^2}}$$

The real-world distribution of light as we get further away from the center of the Petri dish is illustrated in Figure 4.13.

Assumptions for mapping light intensity to radial distance

In our analysis, rather than directly calculating the rate of change of distance with respect to illumination intensity ($\frac{dl}{d\phi}$), we employ an interpolation strategy to estimate the illumination percentage between ϕ_{active} and ϕ_{passive} . This approach is particularly advantageous because it allows us to model the transition of the chemical diode's state from passive to active (and vice versa) without necessitating a precise mathematical mapping of the inverse square law in this context.

Interpolation is mathematically straightforward and significantly practical for our purposes. By defining $\phi_{\text{active}} = 0 \text{ lux}$, representing the absence of light, and $\phi_{\text{passive}} = 24,000 \text{ lux}$, as the maximum light intensity for the diode to remain passive, we create a linear scale between these two points. Thus, any given illumination intensity, ϕ , can be represented as a percentage along this scale:

$$\text{Illumination Percentage} = \frac{\phi - \phi_{\text{active}}}{\phi_{\text{passive}} - \phi_{\text{active}}} \times 100.$$

This formula effectively captures the transition of illumination across the operational range without delving into the complexities of the inverse square law and its derivatives. It succinctly demonstrates how illumination affects the diode's state by positioning any intermediate intensity level within a comprehensible operational range. Such an approach not only simplifies the mathematical analysis but also enhances our intuitive understanding of the system's behavior under varying light conditions.

Assumptions for Light Intensity Calculation

There are assumptions to make when calculating the movable area of the Petri dish in centimeters.

- The area of the Petri dish for a chemical diode is the same as the one for the coincidence detector = 10mm
- The limits (ϕ_{\min} and ϕ_{\max}) are the same for both the coincidence detector and the chemical diode, in reality the coincidence detector has tighter constraints because it's made of diodes and a detector.
- We assume the light bulb is not using soft light, i.e. it has no piece of paper, so the inverse square law accurately describes the light intensity at different distances from the light source.

Calculating the maximum size of the petri dish involves finding the radial distance at which the illumination intensity reaches a specific threshold (ϕ_{\min}) under given conditions. This is shown in Figure 4.14.

- ϕ_{active} and ϕ_{passive} as the active and passive states of illumination intensity.
- ϕ_{\min} as the target illumination intensity.
- h as the height or a relevant physical dimension.

The process involves:

4 Results

1. Calculating the intensity percentage, I_p , as a function of radial distance, r_c , and height, h :

$$I_p(r_c, h) = \frac{1}{\sqrt{1 + \left(\frac{r_c}{h}\right)^2}}$$

2. Interpolating the illumination intensity, ϕ , between ϕ_{active} and ϕ_{passive} based on I_p :

$$\phi(I_p) = \phi_{\text{active}} + (\phi_{\text{passive}} - \phi_{\text{active}}) \cdot I_p$$

3. Finding the radial distance, r_c , where $\phi = \phi_{\min}$, by solving for r_c in:

$$\phi(I_p(r_c, h)) - \phi_{\min} = 0$$

4. Visualizing the relationship between r_c and ϕ , and annotating the plot to highlight the "movable area" and the point where $\phi = \phi_{\min}$.
5. Calculating the maximum circuit size based on the movable area of the Petri dish, where the movable area is the area where the diode limitations are still complied to.

This process determines the radial distance at which a specific illumination intensity (ϕ_{\min}) is achieved, under given conditions.

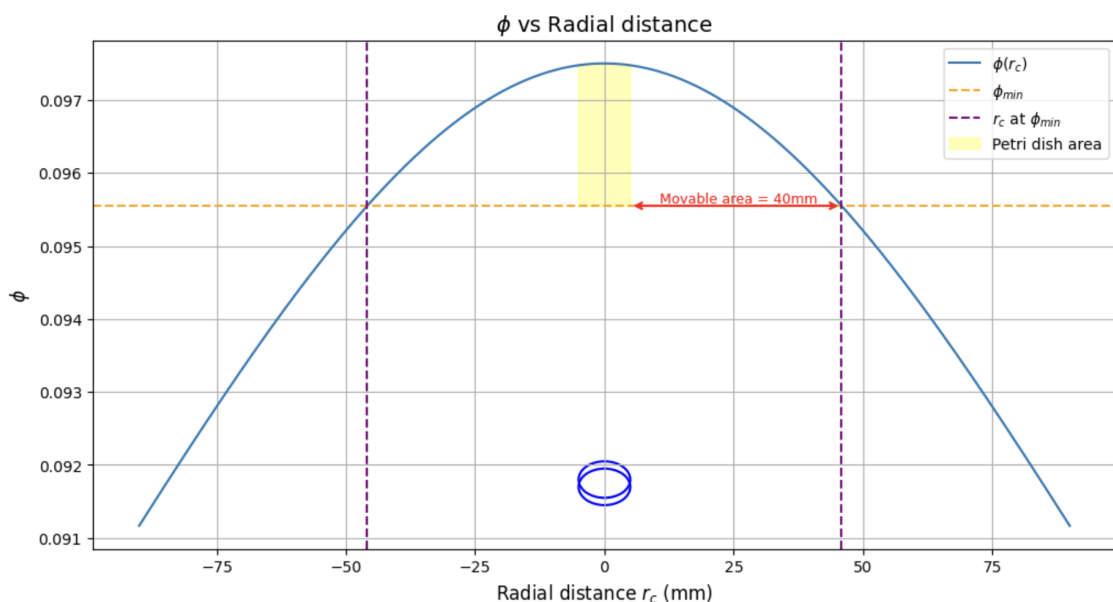


Figure 4.14: The graph illustrates the illumination intensity (ϕ) as a function of radial distance from the center of a Petri dish, represented by an oval at the bottom center. The shaded area within $\pm 10 \text{ mm}$ indicates the physical size of the Petri dish. A movable area of approximately 40.87 mm from the edge of the Petri dish to the radial distance corresponding to ϕ_{\min} is highlighted, demonstrating the operational range within which the chemical diode effectively inhibits the reaction. Beyond this range, the diode becomes non-operational, allowing the reaction to proceed unimpeded.

In this analysis, ϕ_{passive} is defined as the maximum illumination intensity under which the Belousov-Zhabotinsky (BZ) reaction-based chemical diode remains in a passive state,

4 Results

effectively inhibiting the chemical reaction from propagating. The diode operates within this passive state until the illumination intensity decreases to a critical threshold, $\phi_{\min} = 0.09555$. Below this threshold, the diode becomes non-operational and ceases to inhibit the reaction, allowing it to propagate freely. The state of no light, denoted as ϕ_{active} , represents an ideal condition that is not physically achieved in this setup but is simulated using a filter to create the circuit pattern. ϕ_{\min} was chosen based on experimental configurations and literature by Gorecki et al., signifying the operational limit for the diode's passive behavior. This analysis emphasizes the transition from ϕ_{passive} to a non-operational state as light intensity falls below ϕ_{\min} , underscoring the critical operational range for the chemical diode's function in the BZ reaction.

Given the results shown in graph 4.14, the maximum size of the Petri dish for a chemical diode is approximately Given the Petri dish size of 10 mm and extending 35.87 mm in both directions, the maximum chemical circuit size, considering the limitations of ϕ_{\min} and ϕ_{\max} , can be calculated as:

$$\text{Maximum Circuit Size} = 10 \text{ mm} + 40.87 \text{ mm} + 40.87 \text{ mm} = 91.74 \text{ mm}$$

4.6 Light Impact on a CMM Neural Network (Stovold and O'Keefe, 2017)

A CMM neuron is an example of a larger chemical circuit. It is going to serve as an example project for applying the limits found in the previous section. First we need to find the size of the circuit in pixels as reported by Stovold and O'Keefe (2017). In the paper the size of the whole computer is reported as **1998x646px** and uses the exact same configuration as covered in Table 3.1 in Chapter 3.

Using the mapping established in Section 4.2, we can calculate the real-life size of the chemical computer.

Given the dimensions of the circuit in the simulation as 1998×646 pixels and the established scaling factor of 5 px/mm, we can calculate the real-life dimensions of the circuit.

The width and height in real life can be calculated as follows:

$$\begin{aligned}\text{Width in millimeters} &= \frac{\text{Width in pixels}}{\text{Scaling factor}} = \frac{1998 \text{ px}}{5 \text{ px/mm}} = 399.6 \text{ mm}, \\ \text{Height in millimeters} &= \frac{\text{Height in pixels}}{\text{Scaling factor}} = \frac{646 \text{ px}}{5 \text{ px/mm}} = 129.2 \text{ mm}.\end{aligned}$$

Therefore, the real-life dimensions of the circuit are $399.6 \text{ mm} \times 129.2 \text{ mm}$, which corresponds to the minimum size of a petri dish that can accommodate the CMM Neural Network.

Given that the maximum size of the Petri dish for the assumptions in 4.5 and 4.5 is 91.74mm, the CMM Neural Network is too big to have its diode circuits operate within the operational range of the chemical diode. The limits established are minimal limits/soft limits, meaning that the chemical computer in Stovold and O'Keefe (2017) uses much more than diodes and likely has tighter constraints, so if it cannot work under even the minimal limits, it is not going to work under the tighter constraints.

4.7 Light Impact on a single CMM Neuron (Stovold and O'Keefe, 2017)

We established that the big chemical computer in Stovold and O'Keefe (2017) is not possible under the conditions and assumptions established in the previous sections. However, will a single neuron be possible? The size of a single CMM neuron from the paper is not specified, but there is only a design that mentions 200×145 pixels, however it is obvious from the images of the network that the neuron used is smaller and more compact than the designed one. This is why we are going to build a similar neuron and measure it, which is done in Figure 4.15. To calculate the size of the neuron as described by Stovold and O'Keefe (2017), we begin by building a neuron cell that has similar dimensions to the one in the original paper.

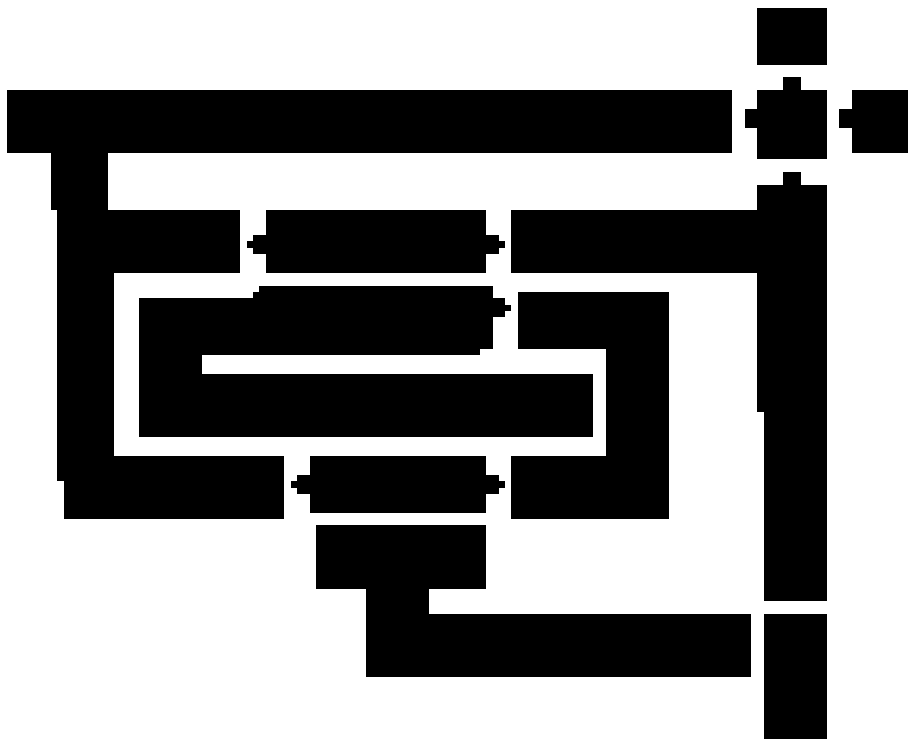


Figure 4.15: Image of a single neuron cell sized at 116x144px built and tested in our simulation, which will be used as a reference for scaling to the approximate size of a single neuron in Stovold and O'Keefe (2017).

The width and height of the neuron in millimeters can be calculated as follows:

$$\text{Width in millimeters} = \frac{\text{Width in pixels}}{\text{Scaling factor}} = \frac{116 \text{ px}}{5 \text{ px/mm}} = 23.2 \text{ mm},$$

$$\text{Height in millimeters} = \frac{\text{Height in pixels}}{\text{Scaling factor}} = \frac{144 \text{ px}}{5 \text{ px/mm}} = 28.8 \text{ mm}.$$

Thus, the real-life dimensions of a single neuron, as adapted from the simulation, are $23.2 \text{ mm} \times 28.8 \text{ mm}$ and are well within the operational range for a chemical diode. However, the assumptions here might not be adequate as the neuron in the paper is likely to have tighter constraints than the chemical diode because it also uses a coincidence detector

4 Results

(AND gate), a cross-junction with diodes that might have different constraints than a single diode due to its compact size and potentially other smaller details that might contribute to shrinking constraints. This is covered in Section 5.2.5.

Also, even if the neuron cell might work under some conditions, that does not mean that it would function correctly as a whole computer because the change in illumination affects propagation times (Reddy et al., 1995) as seen in Section 4.4. Chemical computers have no clock signal and rely heavily on correct signal arrival, so larger circuits like Stovold (2019) might be heavily affected as they rely on propagation to ensure proper arrival of information.

4.7.1 Testing the Custom CMM Neuron with different values of I_p

Manual tests with different ϕ_{passive} values have revealed that the neuron cell is operational at $I_p \geq 0.99$, which means the constraints for the operation are indeed very tight. This is likely due to the AND gate operating under tighter constraints and the compactness of the neuron.

In conclusion it is unclear if the neuron cell can be recreated in the real environment and more investigation is needed.

5 Conclusion & Future work

The project successfully explored the impact of certain imperfections on the performance of chemical computers. The goals in Section 2.6 were mostly achieved and the results were discussed in Chapter 4. The whole chemical computer in Stovold and O'Keefe (2017) was not fully recreated, but a single CMM neuron was and it was measured and discussed in Section 4.7. Light changes and their effect on chemical circuits have been explored to a degree in Sections 4.4 and 4.5, with room for more exploration in Section 5.2.1 and Section 5.2.2.

The results in Section 4.4 and Section 4.5 show that light imperfections like angle of incidence, light source position, light intensity have a significant impact on the performance of chemical circuits.

It was shown that it is very challenging to recreate chemical circuits in real life, as the light source needs to be very uniform and/or the circuit needs to be very small.

5.1 Alternative Light Sources

Gorecki et al. (2003) uses a halogen light bulb as a light source, which is fine for small circuits, but when the circuit grows to the size of what Stovold and O'Keefe (2017) has built, the light source starts to not be enough to illuminate the whole circuit. One way to go around that is to use LED panels that make use of multiple small light sources and a diffuser to make the light more uniform across the whole circuit. That is likely to fully solve the problem of light imperfections and allow for the construction of larger circuits.

5.2 Future Work

5.2.1 Accounting for Light Loss Due to Reflection

The basic idea is that the OHP sheet is not fully transparent, even though it is assumed to be in Gorecki et al. (2003). As the petri dish grows in size, the angle of incidence where the light hits the OHP sheet decreases, leading to more light being reflected away.

Gorecki et al. (2003) includes an opaque material positioned after the OHP sheet to obstruct light, suggesting the necessity of a controlled lighting environment, in order to observe the phenomena using a projector.

Assumptions for Lighting Environment

The external environment in Gorecki et al. (2003) is not described thoroughly, but it is **assumed** to be dim or dark. More specifically, it is assumed to be dark enough that the projector light is the only significant light source in the experiment.

Another role the Overhead Projector (OHP) sheet plays is in the smoothness of the light that is produced after it passes through it due to the diffusion of the light. That

5 Conclusion & Future work

is something unaccounted for in the current simulation and it could affect the results of Section 4.5 because if the light distributes, even though there is less of it, in Gorecki et al. (2003) the experiment still works with this diffused light, so the computer could potentially scale to be slightly larger in size than established in the mentioned section.

To quantitatively model the OHP sheet's impact on light intensity, two primary phenomena are considered: the absorption by the sheet and the light's transmission governed by the angle of incidence. For absorption, the Beer-Lambert Law is applied, while transmission is analyzed through a simplified adaptation of the Fresnel equations.

Fresnel Equations for Transmission

The Fresnel equations (?) determine how much light is transmitted and reflected at an interface, depending on the angle of incidence. For non-polarized light and considering both s-polarized and p-polarized components, the average transmission T can be approximated by:

$$T = \frac{T_s + T_p}{2}$$

where T_s and T_p are the transmission coefficients for s-polarized and p-polarized light, respectively. These coefficients are calculated using the refractive indices of the air (n_1) and the OHP sheet material (n_2), and the angle of incidence θ_i . The Fresnel equations describe the reflection and transmission of light when it hits an interface between two different media. For s-polarized light (electric field perpendicular to the plane of incidence) and p-polarized light (electric field parallel to the plane of incidence), the transmission coefficients can be calculated as follows:

For s-polarized light:

$$T_s = 1 - \left(\frac{n_1 \cos(\theta_i) - n_2 \sqrt{1 - \left(\frac{n_1}{n_2} \sin(\theta_i) \right)^2}}{n_1 \cos(\theta_i) + n_2 \sqrt{1 - \left(\frac{n_1}{n_2} \sin(\theta_i) \right)^2}} \right)^2$$

For p-polarized light:

$$T_p = 1 - \left(\frac{n_2 \cos(\theta_i) - n_1 \sqrt{1 - \left(\frac{n_1}{n_2} \sin(\theta_i) \right)^2}}{n_2 \cos(\theta_i) + n_1 \sqrt{1 - \left(\frac{n_1}{n_2} \sin(\theta_i) \right)^2}} \right)^2$$

where:

- T_s and T_p are the transmission coefficients for s-polarized and p-polarized light, respectively.
- n_1 is the refractive index of the first medium (air, usually close to 1).
- n_2 is the refractive index of the second medium (OHP sheet material).
- θ_i is the angle of incidence.

The average transmission T for unpolarized light can be calculated as the average of T_s and T_p :

$$T = \frac{T_s + T_p}{2}$$

There might be no need to consider polarity as the light is unpolarized and it might be the case that $T_s = T_p$, but it is still good to consider both as there are separate formulas for the calculation of both.

5.2.2 Beer-Lambert Law for Absorption

The Beer-Lambert Law (?) describes how the intensity of light decreases as it passes through an absorbing medium:

$$I = I_0 \cdot e^{-\alpha \cdot l}$$

where:

- I_0 is the initial light intensity before hitting the OHP sheet.
- I is the light intensity after passing through the material.
- α is the absorption coefficient of the OHP sheet material.
- l is the thickness of the OHP sheet.

For our calculations, we assume an absorption coefficient $\alpha = 1 \text{ m}^{-1}$ and a thickness $l = 0.004$ meters (4 mm).

Example Calculation at 45 Degrees Angle of Incidence

At an angle of incidence of 45 degrees, and assuming the refractive index for air as 1.0 and the OHP sheet material as 1.5, we calculate T_s , T_p , and the average transmission T . The transmission coefficients reflect how much of the incident light is transmitted through the OHP sheet at this angle.

Using these Fresnel equations, we account for the angle-dependent transmission of light through the OHP sheet, complementing the Beer-Lambert Law used to calculate the light intensity after absorption by the material.

At a 45-degree angle of incidence, we calculated the transmission coefficients for s-polarized and p-polarized light, and found the average transmission T to be approximately 0.950. This indicates that about 95% of the light is transmitted through the OHP sheet at this angle.

Combining the effects of absorption and transmission, the final intensity I_{final} of light after passing through the OHP sheet and considering the angle of incidence is given by:

$$I_{\text{final}} = I_0 \cdot e^{-\alpha \cdot l} \cdot T$$

Substituting the given values and assumptions, we find:

$$I_{\text{final}} \approx 0.946$$

This result indicates that the combined effect of slight absorption by the OHP sheet and the reduction in transmission due to the 45-degree angle of incidence leads to a final light intensity of approximately 94.6% of the initial intensity.

These calculations demonstrate the importance of considering both material properties and geometric factors, such as the angle of incidence, when modelling the transmission of light through materials in experimental setups.

5.2.3 Examining the Impact of Spike on Diode Robustness

Section 4.3.2 examines the how light variations impact the operation of a diode. However, this diode has a spike that helps it become more robust to these variations. It would be interesting how much the range ϕ_{\min} to ϕ_{\max} would decrease by removing the spike from the diode.

5.2.4 Accounting for the Change on ϕ_{active}

In order to simulate the environment becoming darker in Section 4.4, the value of ϕ_{passive} is decreased. It would be interesting to see if it is necessary to modify the value of ϕ_{active} as well using some relationship between ϕ_{passive} and ϕ_{active} . It is also entirely possible that they are not related because ϕ_{active} represents a state of null illumination or total darkness that allows the reaction to happen, while ϕ_{passive} is a baseline illumination given by the light bulb that is used to shine light onto the circuit. That is a constant value and would not change as we travel through the surface of the petri dish, while ϕ_{passive} changes because it directly represents less light and starts approaching the value of ϕ_{active} as the light becomes dimmer and the reaction becomes more active.

5.2.5 Accounting for Other Chemical Component Limitations Than Diodes

Section 4.5 only considers the limitations of the diodes in the chemical computer. Larger circuits like the ones used in Stovold and O'Keefe (2017) use multiple other elements like a coincidence detector (AND gate) and other details. It was established that the limits for a diode (ϕ_{\min} and ϕ_{\max}) for the value of ϕ_{passive} are 0.106127 and 0.106127, respectively. Observations in Section 4.7.1 show that the value of I_p is around 0.99 in order to allow for the full neuron cell to operate normally. This would mean that the values would be a lot closer to $\phi_{\text{literature}}$, but the exact values are not calculated here. In order for one to calculate them, they can use the mathematical formulas used in Section 4.3 and apply them to find the values of ϕ_{\min} and ϕ_{\max} for the CMM neuron by going 1% in both directions.

Bibliography

- Adamatzky, A. (2019), ‘A brief history of liquid computers’, *Philosophical Transactions of the Royal Society B* **374**(1774), 20180372.
- Adamatzky, A., Costello, B. D. L. and Asai, T. (2005), *Reaction-diffusion computers*, Elsevier.
- Barry, A. L., Coyle, M. B., Thornsberry, C., Gerlach, E. and Hawkinson, R. (1979), ‘Methods of measuring zones of inhibition with the bauer-kirby disk susceptibility test’, *Journal of clinical microbiology* **10**(6), 885–889.
- Cui, J. (2004), *Synchronization of spatiotemporal patterns and modeling disease spreading using excitable media*, West Virginia University.
- De Kepper, P. and Epstein, I. R. (1982), ‘Mechanistic study of oscillations and bistability in the briggs-rauscher reaction’, *Journal of the American Chemical Society* **104**(1), 49–55.
- Dittrich, P. (2004), Chemical computing, in ‘International Workshop on Unconventional Programming Paradigms’, Springer, pp. 19–32.
- Edge, C. (2020), ‘Messing around in parameter space’, YouTube. Available: <https://www.youtube.com/watch?v=4m6mdFfeQMI> [Accessed: (Oct 26, 2023)].
- Edwards (1970), *Physics for O.N.C. Courses*, Elsevier. Chapter 25 - Illumination and Photometry (Pages 473-495).
- Field, R. J. (2007), ‘Oregonator’, *Scholarpedia* **2**(5), 1386.
- Fujilamp (2024), ‘Datasheet for jdc 100v 300w’, http://www.fujilamp.com/html/catalogue_e/jcd_e.html.
- Gorecki, J., Yoshikawa, K. and Igarashi, Y. (2003), ‘On chemical reactors that can count’, *The Journal of Physical Chemistry A* **107**(10), 1664–1669.
URL: <https://doi.org/10.1021/jp021041f>
- Kuhnert, L., Agladze, K. and Krinsky, V. (1989), ‘Image processing using light-sensitive chemical waves’, *Nature* **337**(6204), 244–247.
- Reddy, M. R., Dahlem, M., Zykov, V. and Müller, S. (1995), ‘The effect of an illumination jump on wave propagation in the ru-catalyzed belousov-zhabotinsky reaction’, *Chemical physics letters* **236**(1-2), 111–116.
- Stone, C., Toth, R., de Lacy Costello, B., Bull, L. and Adamatzky, A. (2008), Coevolving cellular automata with memory for chemical computing: Boolean logic gates in the bz reaction, in ‘Parallel Problem Solving from Nature—PPSN X: 10th International Conference, Dortmund, Germany, September 13-17, 2008. Proceedings 10’, Springer, pp. 579–588.

Bibliography

- Stovold, J. (2019), ‘Rdcsim: a gpu-accelerated, interactive simulator for reaction–diffusion chemistry’.
- Stovold, J. and O’Keefe, S. (2017), ‘Reaction–diffusion chemistry implementation of associative memory neural network’, *International Journal of Parallel, Emergent and Distributed Systems* **32**(1), 74–94.
- Toth, R., Stone, C., Adamatzky, A., de Lacy Costello, B. and Bull, L. (2009), ‘Experimental validation of binary collisions between wave fragments in the photosensitive belousov–zhabotinsky reaction’, *Chaos, Solitons & Fractals* **41**(4), 1605–1615.
URL: <https://www.sciencedirect.com/science/article/pii/S0960077908003032>
- Toth, R. and Taylor, A. F. (2006), ‘The tris (2, 2'-bipyridyl) ruthenium-catalysed belousov–zhabotinsky reaction’, *Progress in Reaction Kinetics and Mechanism* **31**(2), 59–115.
- Turing, A. M. (1952), ‘The chemical basis of morphogenesis’, *Philosophical Transactions of the Royal Society of London B* **237**(641), 37–72.
- Yamada, Y., Ito, H. and Maeda, S. (2022), ‘Artificial temperature-compensated biological clock using temperature-sensitive belousov–zhabotinsky gels’, *Scientific reports* **12**(1), 22436.
- Zambrano, A., Zadorin, A. S., Rondelez, Y., Estévez-Torres, A. and Galas, J.-C. (2015), ‘Pursuit-and-evasion reaction-diffusion waves in microreactors with tailored geometry’, *The Journal of Physical Chemistry B* **119**(17), 5349–5355. PMID: 25839240.
URL: <https://doi.org/10.1021/jp509474w>

A Original Project Proposal

A.1 Aims & Objectives

A.1.1 Aims

The aim of the project is to create one of these BZ simulations and add a number of imperfections, measuring how they impact the simulation. These imperfections would typically be found in the real world in the form of dust particles, terrain obstacles or other environmental factors.

The main idea is to create an application using Flutter and to simulate the reaction.

1. Interactive Simulation App Development with Flutter Flutter is a mobile application framework that allows for easy addition of elements of interactivity and allows for lower level control over pixels, which is necessary for creating one of these simulations. The reason for choosing Flutter as opposed to another framework or solution is because of the already present familiarity with the framework.

The simulation shall run on the GPU, so addressing the GPU usage is crucial. The current solutions are to use the recently added `flutter_gpu` package or integrating Dart Foreign Function Interface (FFI) to run native shaders.

2. Creating a game from the simulation. Since the project is focused around imperfections, it could be possible to let the user play with or against the waves (see figure ??) using the `flame` package (minimal game engine).

The simulation has illumination that creates a path, the aim is to create a game where the user has to run away from the waves, but is also constrained to the illuminated area, so for example a single wave could split and then catch the player from both directions.

3. Adding imperfections: One of the main themes of the project is finding imperfections. The goal is to let the player defend himself from the waves using imperfections in the simulation that impact the reaction-diffusion model. This could mean throwing dust particles at the wave or adding temperature to the model that speeds up or slows down the reaction at a particular zone, so that a part of the waves travels more slowly, disrupting the reaction. The aim is to allow the user to only use imperfections as a means of defence.

A.1.2 Challenges

Among the challenges I might face I see myself running into a computational problem where dt , being as small as it is, could force me to run the simulation at a very slow rate, which then would make me increase the speed at which it is run, using more CPU, but since the project is *real time*, I cannot afford to go beyond the maximum allowed CPU per frame or I would cause jitter, running code on the GPU should help, but there also needs

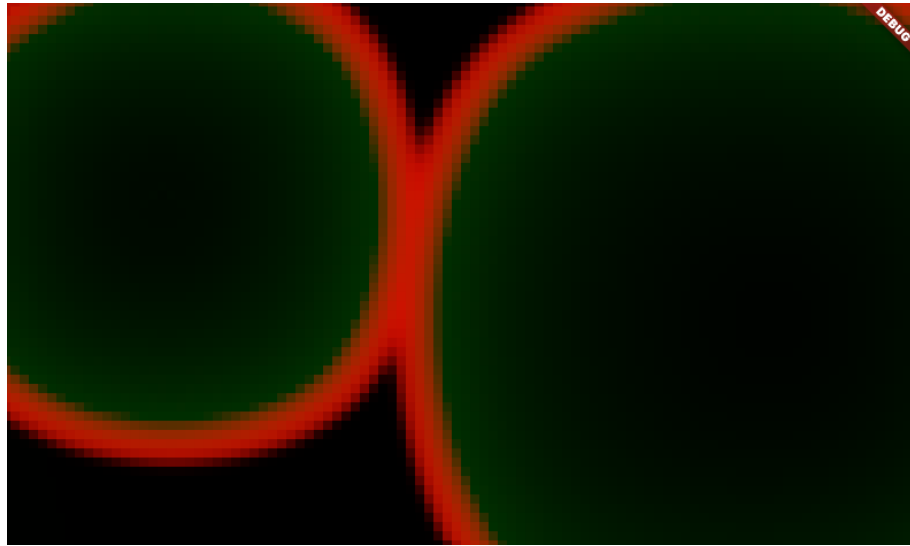


Figure A.1: Expanding wave pattern from this project using the Oregonator model

to be a way to only perform these calculations on a subset of the whole map. Also if this were a game, there could be beacons generating these waves that the user has to destroy. Flutter also has a 2D game engine that I've wanted to explore and that could be a great opportunity. The other reaction-diffusion systems are very scientific or are presented as a video. Zambrano et al. (2015) have used reaction and diffusion to find the shortest path in a maze.

A.2 Related work

The area of reaction-diffusion simulations has been explored well. The simulations of waves are used to produce computing units like counters and logic gates (Gorecki et al., 2003) as well as neurons (Stovold, 2019).

Edge (2020) has created a game (figure A.2) out of the Gray-Scott model where ships battle inside of a goo-like substance and the chemical acts as a dynamic obstacle. The game looks of very high quality despite the lack of interest from the public. Other than this project, there isn't a lot of interest in the joint field of reaction-diffusion simulations and gaming

A.3 Methodologies

1. The project is going to use an agile iterative approach where the phases of the Software Development Life Cycle are performed every sprint.
2. It's important is that the work is broken down into chunks according to the SMART task framework, which stands for Specific, Manageable, Achievable, Relevant, Time-bound. It's important for the tasks to be small and understandable, without any dependencies to other tasks
3. If one task requires the parallel completion of another task, then these tasks should be the same task with two things to do in the task.

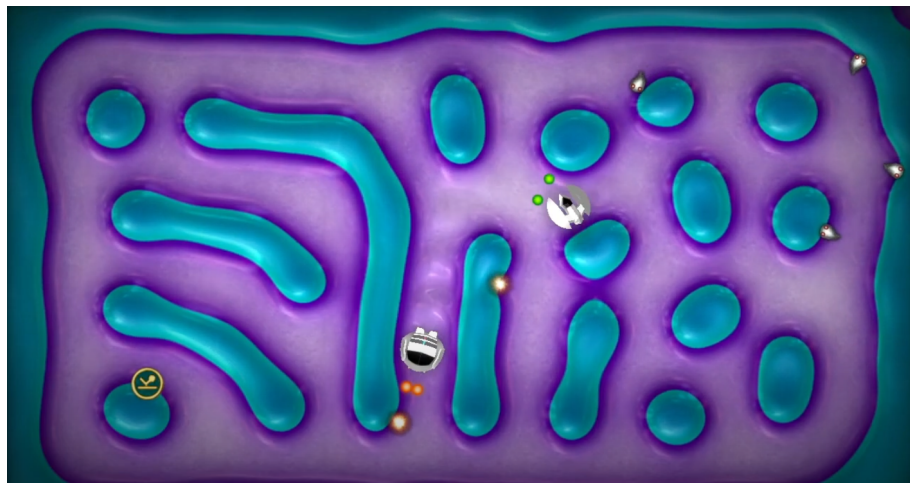


Figure A.2: Reaction Diffusion Game by Chaotic Edge

4. The project is going to use ClickUp as a Project Management System (PMS) due to its flexibility and integration with calendar and task management apps.
5. The most important task management tool to be used in this project is Reclaim.AI, which uses priorities and deadlines to auto schedule your calendar based on your preferences and hours, it has an integration with the most popular PMSs like Jira, ClickUp, Asana, etc.
6. The Project Management System tasks are going to use custom statuses:
 - a) TODO - feature not started
 - b) RESEARCHING - gathering information and reading about feature
 - c) SUBTASKING - feature clear. creating subtasks and checklists to make task execution easier
 - d) IMPLEMENTING - implementing feature
 - e) TO PRESENT - feature implemented. Waiting to be presented to supervisor
 - f) FOR REVISION - supervisor left feedback. Return task to RESEARCHING or IMPLEMENTING
7. The project is going to use the 1 week sprints to divide work into even blocks of work if the backlog ends up being too big. If the backlog remains small, the project is going to use the backlog and not use sprints.

A.4 Programme of Work

The project, being agile, doesn't have strong formal phases, it follows an iterative approach. There are however distinct phases in the planned development of this project (see figure A.3):

1. Planning & Analysis - this phase is going to specify goals of the sprint
2. Design - The project is going to be designed in more detail, that includes library choices, design choices, etc

A Original Project Proposal

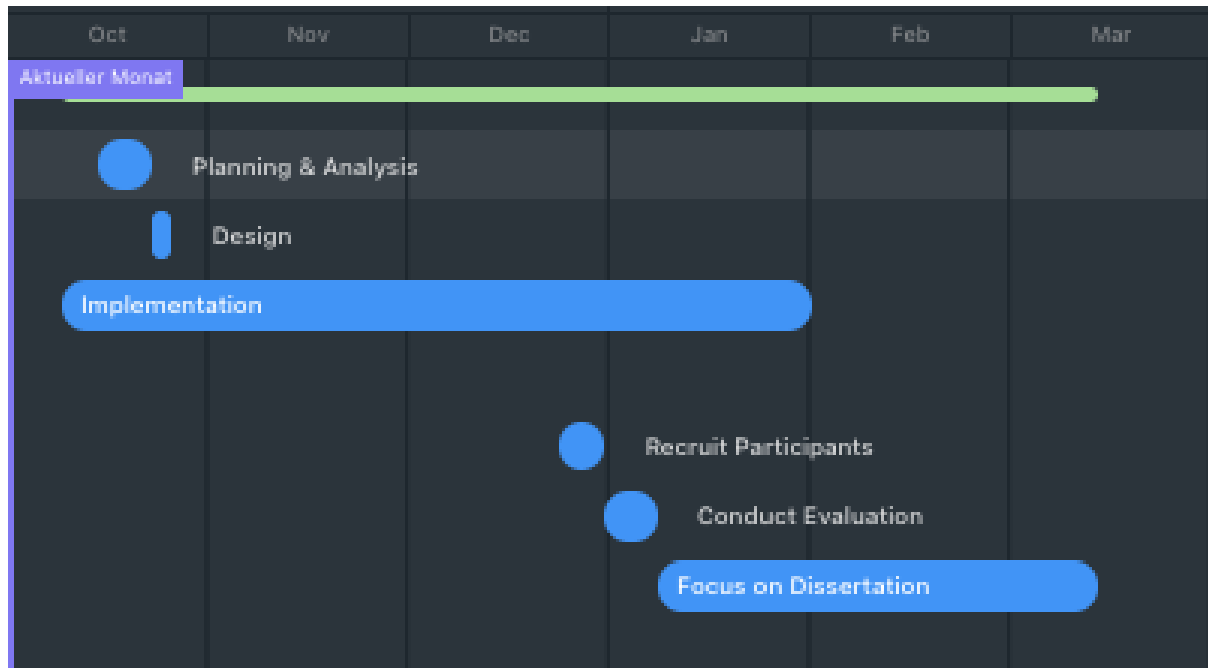


Figure A.3: Gantt Chart

3. Implementation - This phase would take up the majority of the sprint time
4. Testing - last phase before the project transitions into a finalising state
5. Searching for Participants - a stage where about 5 people need to be recruited to perform evaluation
6. Conduct evaluation - the evaluation is going to be performed using heuristics, for example how intuitive the game is, etc.
7. Focus on dissertation - time to shift focus on using the resources and documentation to create the dissertation.

This project is prototypical, so it's going to have reduced planning and design phases.